Optics Communications 284 (2011) 3669–3692

Contents lists available at ScienceDirect

Optics Communications

journal homepage: www.elsevier.com/locate/optcom

Ultrafast optical pulse shaping: A tutorial review

Andrew M. Weiner

Purdue University, School of Electrical and Computer Engineering, West Lafayette, IN 47907–1285, United States

ARTICLE INFO

Article history:
Received 28 March 2011
Accepted 30 March 2011
Available online 15 April 2011

Keywords:
Ultrafast optics
Pulse shaping
Femtosecond optics
Coherent control
Optical signal processing
Radio-frequency photonics

ABSTRACT

This paper presents a tutorial on the field of femtosecond pulse shaping, a technology that enables generation of nearly arbitrary, user defined, ultrafast optical waveforms, with control of phase, amplitude, and polarization. The emphasis is on Fourier transform pulse shaping, the most widely applied technique. Selected pulse shaping applications are described, with specific discussion of coherent control of quantum and nonlinear processes and of lightwave communications. Two new areas of pulse shaping research, namely, hyperfine spectral resolution pulse shaping and pulse shaping applications in ultrabroadband RF photonics, are discussed and illustrated with examples taken from the author's laboratory.

1. Introduction

Ultrafast optics technology is now widespread. Pulses are routinely generated on the picosecond and femtosecond time scales, and active investigation of the attosecond time scale, based on highly nonlinear frequency conversion of femtosecond sources into the soft X-ray spectral region, is under way. Although mode-locked lasers are by far the most common source of ultrashort pulses, especially in the deep femtosecond regime, other generation approaches, based for example on strong electro-optic phase modulation and subsequent compression of continuous-wave lasers, are attracting increasing attention as well. The application space for ultrashort pulses has become extremely broad, including but not limited to high-field laser-matter interactions, ultrafast time-resolved spectroscopy, high precision frequency metrology and development of optical clocks, machining and processing of materials, nonlinear microscopy, optical communications, and radio-frequency signal processing. Texts providing comprehensive treatments of ultrafast optics technology may be found, for example, in Refs. [1,2].

In this tutorial review article, we focus on pulse shaping methods that enable programmable reshaping of ultrafast pulses, or generation of arbitrary optical waveforms, according to user specification. Pulse shaping and processing technologies are complementary to ultrashort pulse generation and characterization methods and are now widely applied, both in ultrafast optical science and in ultrafast technology. Examples of application areas for pulse shaping include pulse compression in the few cycle regime, dispersion compensation for fiber optic communications, coherent laser control of quantum mechanical processes, and spectrally selective nonlinear microscopy, to name a few.

We concentrate in this article on the most widely adopted pulse shaping method, in which waveform synthesis is achieved by spatial masking of the spatially dispersed optical frequency spectrum. A key point is that because waveform synthesis is achieved by parallel modulation in the frequency domain, waveforms with effective serial modulation bandwidths as high as terahertz and above can be generated without requiring any ultrafast modulators. We will be particularly interested in pulse shaping using spatial light modulators (SLMs), where the SLM allows reprogrammable waveform generation under computer control. Another popular pulse shaping technology, termed the acousto-optic programmable dispersive filter, which accomplishes similar ends but with a quite different implementation based on a co-propagating acousto-optic interaction, is also discussed in this article. A review article by Froehly describes a variety of pulse shaping techniques investigated prior to 1983 for picosecond pulses [3]. A comprehensive review of programmable pulse shaping written by the current author may be found in [4], while [5] provides a very recent survey of both programmable pulse shaping technologies and applicable pulse characterization techniques. Other early reviews include Ref. [6], which provides a broad account of signal processing techniques for ultrashort pulses (including pulse shaping), and Ref. [7], which describes initial results on femtosecond pulse shaping using fixed masks and related experiments on picosecond pulse shaping performed in the context of nonlinear pulse compression. Additional reviews focus on specific application areas of pulse shaping, including coherent and quantum control [8–10] and "information optics" for communications and pulse processing [11–13].

Due to space limitations, several interesting methods for optical pulse shaping and manipulation are not included in this article. These include the so-called direct space-to-time pulse shaping technique [14–18] and a variety of pulse processing techniques that employ

E-mail addresses: amw@purdue.edu, ddexter@purdue.edu.

0030-4018/$ – see front matter © 2011 Elsevier B.V. All rights reserved.
doi:10.1016/j.optcom.2011.03.084

large amounts of dispersion and chirp, including temporal imaging systems based on clever combinations of dispersion and phase modulation [19,20]. An introduction to these approaches may be found in chapter eight of Ref. [1].

The remainder of this article is organized as follows. Section 2 introduces the basics of Fourier transform pulse shaping, including the experimental arrangement and examples of waveforms generated via this technique. Key ideas from pulse shaping theory are summarized in Section 3. Section 4 focuses on technologies for programmable pulse shaping, including both liquid crystal and acousto-optic spatial light modulators. Compared to this author's earlier review of programmable pulse shaping [4], new material on liquid crystal on silicon (LCoS) SLMs, which offer radically increased numbers of pixels, is now included, as is discussion of acousto-optic programmable dispersive filters. Section 5 begins with an overview of control strategies for pulse shaping and then surveys pulse shaping applications, focusing on examples in coherent control of nonlinear and quantum mechanical processes and in lightwave communications. The applications selected represent examples of "open-loop" pulse shaping control which lend themselves to intuitive understanding. Sections 6 and 7 cover two frontier areas in pulse shaping, with examples drawn primarily from work in the author's laboratory. In particular, Section 6 concerns pulse shaping with high spectral resolution, emphasizing experiments in which pulse shaping and frequency comb technologies are brought together. The combination of high temporal coherence provided by frequency comb sources and high temporal resolution control provided by pulse shaping provides new signal generation and applications opportunities not previously available. Section 7 covers examples of ultrabroadband radio-frequency (RF) photonics, a relatively new discipline in which high-speed photonics technologies, including pulse shaping, aid in the generation and processing of RF electromagnetic signals with instantaneous bandwidths beyond the capabilities of conventional electronics solutions. Finally, in Section 8 we conclude.

2. Optical pulse shaping basics

Fig. 2.1 shows the basic setup for Fourier transform optical pulse shaping, a widely adopted approach in which powerful Fourier synthesis methods are utilized to generate almost arbitrarily shaped femtosecond optical waveforms [4,21]. The key idea is that the incident femtosecond pulse is first decomposed into its constituent spectral components by a spectral disperser (usually a grating) and a focusing element (a lens or a curved mirror). A spatially patterned mask then modulates the phase and amplitude, and sometimes the polarization, of the spatially dispersed spectral components. After the spectral components are recombined by a second lens and grating, a shaped output pulse is obtained, with the pulse shape given by the Fourier transform of the pattern transferred by the mask onto the spectrum. An important point is that this so-called 4*f* pulse shaping arrangement is ideally free of temporal dispersion [22]; therefore, in the absence of a pulse shaping mask, the output pulse is ideally identical to the input. Pulse shaping masks were originally implemented by using microlithographic patterning techniques [21] and subsequently by using programmable spatial light modulators [4,23–25], acousto-optic modulators [26], holographic masks, deformable mirrors [27], and micro-mirror arrays. Most commonly, pulse shaping is implemented using programmable liquid crystal modulator arrays [4,23–25] that allow independent, simultaneous gray-level control of both spectral amplitude and phase. Using pulse shaping methods, femtosecond pulses can be engineered into complex optical signals, almost arbitrarily and according to specification. A key point is that waveform synthesis is achieved by parallel modulation in the frequency domain, which is achieved by spatial modulation of the dispersed optical frequency spectrum. Thus, waveforms with effective serial modulation bandwidths as high as hundreds of terahertz can be generated and manipulated, without requiring ultrafast modulators.

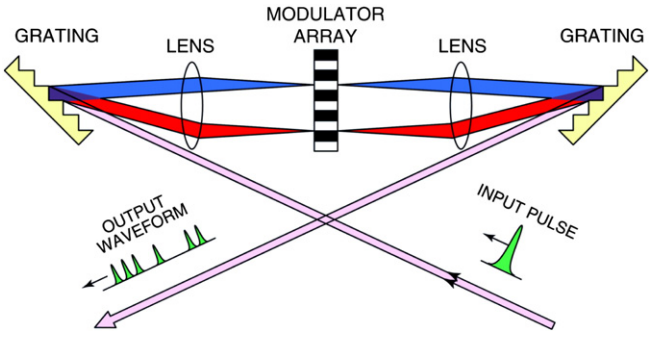

Fig. 2.1. Basic setup for Fourier transform optical pulse shaping.

Fig. 2.2 shows several examples of shaped pulses generated in the author's laboratory. In each of these examples, experiments were performed using ~100 fs duration input pulses. Shaped pulses were measured by nonlinear mixing with unshaped reference pulses (directly from the laser) in a second harmonic crystal. Recording the second harmonic output as a function of reference delay yields an intensity cross-correlation trace [1], which for a sufficiently short reference pulse provides a good likeness of the shaped pulse intensity as a function of time. This technique may be considered the optical equivalent of sampling oscilloscopes widely used for measurement of fast electronic signals. Fig. 2.2(b) shows an ultrafast optical square pulse, in which the spectrum is patterned according to a sinc-function [21]. The intensity profile exhibits an ~2-ps, approximately flat-topped region, with fast rise and fall times consistent with the original 100 fs pulse duration. The overshoot and ringing arise from truncation of the sinc-function spectrum at finite bandwidth and are expected. Fig. 2.2(a) shows a femtosecond "data packet," in which the single input pulse is reshaped into a sequence of evenly spaced pulses, with eight pulses on and one pulse missing [28]. The pulse spacing is approximately 400 fs, corresponding to peak data rate of 2.5 Tb/s, far beyond the modulation capabilities of electronic approaches. An interesting point in this example is that because the phase of individual pulses in the output waveform was not specified, it was possible to accomplish the pulse shaping using manipulation of spectral phase alone.

Although control of both spectral amplitude and phase is required for general pulse shaping operations, it is the spectral phase that arguably has the most fundamental impact on temporal waveforms. Eq. (2.1) highlights an important and fundamental relationship

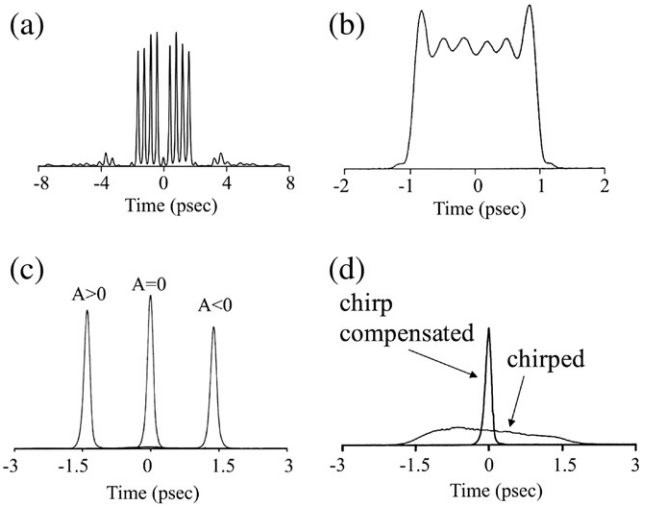

Fig. 2.2. Pulse shaping examples. (a) Femtosecond data packet. (b) ultrafast square pulse. (c) Pulse position modulation resulting from linear spectral phase. (d) Chirping and compression resulting from quadratic spectral phase.

between frequency dependent delay $\tau(\omega)$ and frequency dependent phase $\psi(\omega)$ [1]:

$$\tau(\omega) = \frac{-\partial\psi(\omega)}{\partial\omega} \tag{2.1}$$

Fig. 2.2(c) gives data from experiments in which a liquid crystal modulator array was programmed for a spectral phase linear in frequency, $\psi(\omega) = A(\omega - \omega_o)$. According to Eq. (2.1), this corresponds to a uniform shift in pulse delay. The three traces shown in Fig. 2.2(c) correspond to experiments in which the slope of the phase function (the A parameter) was set to be positive, zero, or negative, respectively. This results in output pulses that are either shifted many pulse widths earlier in time, that remain unshifted, or are shifted many pulse widths later in time [24]. A quadratic phase function, $\psi(\omega) = B(\omega - \omega_o)^2$, is another important case. According to Eq. (2.1), the corresponding frequency dependent delay is linear in frequency. Fig. 2.2(d) shows an example in which the input pulse is intentionally chirped, i.e., it possesses an approximately linear frequency dependent delay. By using the pulse shaper to apply an appropriate quadratic phase (equal and opposite to that present on the input pulse), the pulse is compressed to the bandwidth limit [24]. An important point is that the pulse shaper provides the flexibility to impose arbitrary spectral phase functions, including nearly arbitrary superpositions of quadratic, cubic, and higher order spectral phase. This capability has substantial utility in compensation of dispersion and chirp, with applications ranging from fiber optic dispersion compensation to optimized compression of pulses in the single-cycle regime and of high power pulses from chirped pulse amplifier systems.

In practice, there are many variations in which the so-called 4*f* pulse shaping arrangement of Fig. 2.1 is implemented. The setup is also frequently implemented in a reflection geometry, in which a mirror placed after the spatial mask directs the field back through the first lens and grating [29]. The reflection geometry substantially simplifies the optical alignment procedure for fiber optic applications, in which light must be coupled with low loss out of and back into single-mode optical fiber. There are also several choices of spectral disperser. Although diffraction gratings are the most common, arrayed waveguide gratings, virtually imaged phased arrays (VIPA etalons), and prisms have also been used. Arrayed waveguide gratings, a well known technology for multiplexing or demultiplexing different wavelengths in wavelength-division multiplexed (WDM) optical communications, have been adapted to realize pulse shapers on a chip based on multi-channel thermo-optic amplitude and phase control [30–32]. VIPAs, optical elements that marry the high spectral resolution potential of etalons with the spectral disperser functionality of gratings [33], have been applied to realize pulse shapers with very high spectral resolution (<1 GHz, much finer than the tens or hundreds of GHz spectral resolution typical for grating based pulse shapers) [34,35] — see Section 6. On the other hand, in order to avoid the overlap of multiple diffraction orders, prism-based pulse shapers have been utilized for applications involving extremely broadband pulses approaching the single-cycle regime [36,37]. Also for pulse durations below a few tens of femtoseconds, it is common to build pulse shapers using curved mirrors as focusing elements in order to avoid effects arising from the chromatic dispersion of lenses [38].

For femtosecond applications pulse shaping is most commonly used to operate on pulses derived from mode-locked lasers. However, there are many other possibilities. For example, prism-based pulse shaping has been exploited to compress multi-octave Raman frequency combs into periodic waveforms approximately a single optical cycle in duration [36]. Pulse shaping optics have also been adapted for manipulation of WDM communication signals, in which there is no fixed phase relationship between different wavelength channels. In this case the pulse shaper operates on the spectral intensity only. Resulting devices such as spectral gain equalizers and wavelength-selective switches are available as commercial products and are deployed in lightwave communications networks — see Section 5.2 for further discussion. Pulse shaping may also be applied to incoherent light sources. Fig. 2.3(a) illustrates the setup of an experiment in which amplified spontaneous emission (ASE) from an erbium-doped fiber amplifier is manipulated by a pulse shaper [39]. Although it is not possible to generate a deterministic intensity profile from such a noise source, it is still possible to reshape the noise. This can be observed by placing the pulse shaper in one arm of an interferometer — leading to the ability to shape the electric field cross-correlation function between the original and reshaped noise. Fig. 2.3 (b–d) show interferograms measured with the pulse shaper either quiescent or programmed for different values of linear spectral phase. The shape of the interferograms are all equal to the inverse Fourier transform of the optical power spectrum [1], but are shifted along the delay axis according to the slope of the spectral phase, exactly as described earlier for coherent pulses. Shaping may even be applied to nonclassical light sources. Reference [40] reports an experiment involving an entangled photon source based on parametric down-conversion. In this experiment the pulse shaper was used to achieve user defined reshaping of the two-photon wave function, which was observed through an ultrafast coincidence detector implemented via sum frequency generation.

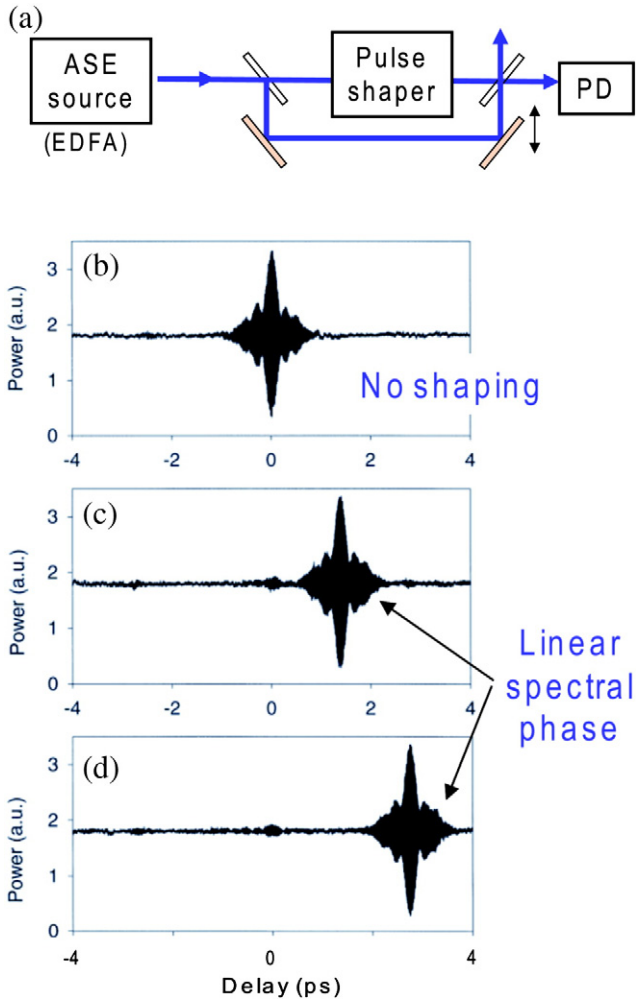

Fig. 2.3. Pulse shaping with broadband incoherent light: manipulation of the electric field cross-correlation function. (a) Experimental schematic. (b–d) Electric field cross-correlation traces with (b) flat phase or (c–d) different values of linear spectral phase.

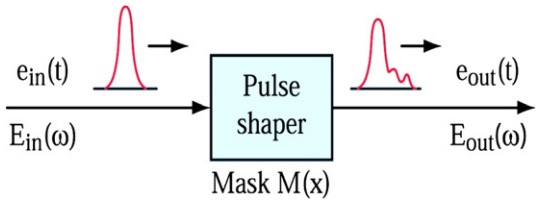

Fig. 3.1. Block diagram view of pulse shaping: idealized representation with perfect spectral resolution.

3. Results from pulse shaping theory

A detailed theoretical analysis of pulse shaping is given in reference [1]. Here we will confine our discussion to a few important points. At the simplest level we may envision pulse shaping operation as illustrated in Fig. 3.1. An input pulse, with complex amplitude functions in the time and frequency domains denoted $e_{in}(t)$ and $E_{in}(\omega)$, respectively, passes through a pulse shaper with spatial mask $M(x)$. $M(x)$ is taken to be complex to represent both intensity and phase filtering. The output field in the spectral domain is written

$$E_{out}(\omega) = M(\alpha\omega)E_{in}(\omega), \tag{3.1}$$

where $\alpha = \partial x/\partial\omega$ is the spatial dispersion at the masking plane. In this description of the pulse shaper, the output spectrum is given by the input spectrum multiplied by a complex frequency response function equal to a directly scaled version of the mask. The approximation of linear spectral dispersion is usually a good one for grating-based pulse shapers with pulse durations greater than a few tens of femtoseconds. (Some new effects arising when the linear spectral dispersion approximation does not fully hold are discussed, for example, in [41].) The output field in time is obtained from the inverse Fourier transform of Eq. (3.1):

$$e_{out}(t) = e_{in}(t) * m(t/\alpha) \tag{3.2}$$

where

$$m(t/\alpha) = \frac{1}{2\pi}\int M(\alpha\omega)e^{j\omega t}d\omega. \tag{3.3}$$

The output field is given by the input field convolved with the impulse response function of the pulse shaper, which is equal to the inverse Fourier transform of the scaled masking function. An important point is that for a transform-limited input pulse, pulse shaping generally does not decrease the pulse duration, as bandwidth is not increased.

In reality, the situation is not quite so simple. As sketched in Fig. 3.2, important effects arise because the field corresponding to any single optical frequency component occupies a finite spot at the masking plane. Fig. 3.2(inset) illustrates diffraction of a single frequency field encountering a mask with an abrupt spatial feature; however, the following discussion applies as well for masks with gradual rather than abrupt features. The point is that unless the focused spot is infinitely small, spatial variation in the mask, in conjunction with diffraction, fundamentally reshapes the spatial field of any particular frequency component. Furthermore, different frequencies impinge on different locations of the mask and therefore experience different spatial reshaping. As sketched in Fig. 3.2, this means that the field after the pulse shaper will be a coupled function of space and time (equivalently of space and frequency). The form of the coupled space-time field is worked out in [42]. However, for most practical applications, one wishes to generate an output field that is shaped in time in a way that is independent of the spatial coordinates. This can be realized by using an appropriate spatial filter. In the desirable case where the spatial filter actually selects a fundamental Gaussian spatial mode matched to the unshaped field (this can be implemented by coupling into a single mode fiber for applications in lightwave, or by coupling into a cavity for applications involving a regenerative amplifier), the shaped output field becomes [1,43]:

$$E_{out}(\omega) \sim \left[\int dx\, M(x)\exp\left[-2(x-\alpha\omega)^2/w_o^2\right]\right] E_{in}(\omega) \tag{3.4}$$

where w_o is the radius of the assumed Gaussian field focused at the masking plane. A key point is that the masking function is smeared according to the finite spot size. This imposes a minimum feature size that can be transferred from the mask onto the spectrum. This results in a minimum spectral resolution, which is similar in origin to that of a conventional spectrometer. The time domain field, obtained via inverse Fourier transform of Eq. (3.4), is written

$$e_{out}(t) \sim e_{in}(t) * \left[m(t/\alpha)\exp\left(-w_o^2 t^2/8\alpha^2\right)\right]. \tag{3.5}$$

Now the output field is equal to the input field convolved with a modified pulse shaper impulse response function. The modified impulse response function is equal to the infinite spectral resolution impulse response function $m(t/\alpha)$ multiplied by a Gaussian window function. The finite spot size and resulting finite spectral resolution restrict pulse shaping operation to a finite time aperture.

These results are summarized by Fig. 3.3. Fig. 3.3(a) shows a sketch of a spectrum with bandwidth B, which we assume represents the bandwidth of the input pulse, and minimum feature size δf, which is limited either by the smallest spatial feature on the mask or by the spectral resolution of the pulse shaper, whichever is smaller. Fig. 3.3 (b) shows a sketch of a possible corresponding temporal intensity profile, with minimum feature duration δt and time window T. The shortest temporal feature that can be realized is inversely related to

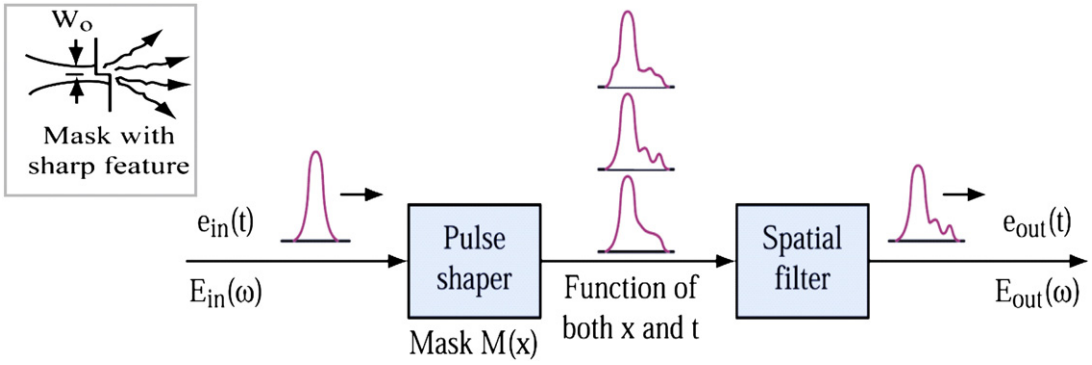

Fig. 3.2. Block diagram view of pulse shaping: more realistic representation in which spatial variation of the pulse shaping mask (inset at left) together with finite spectral resolution gives rises to spatially dependent shaped fields.

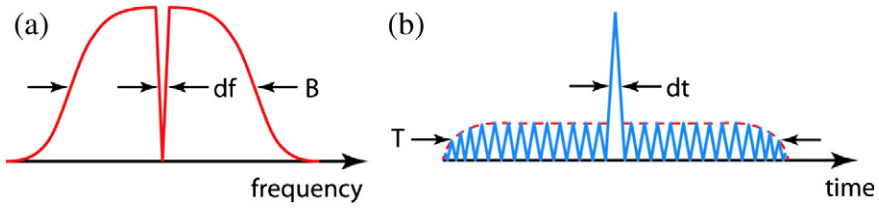

Fig. 3.3. Schematic view of pulse shaping (a) in frequency domain and (b) in time domain.

the total bandwidth, $B\cdot\delta t \approx 0.44$, and the maximum temporal window is inversely related to the finest achievable spectral feature, $\delta f\cdot T \approx 0.44$. Here Gaussian shapes are assumed, and all pulse durations and bandwidths refer to full width at half maxima. The time-bandwidth product (BT) of the shaped pulse is equal to the number of independent features that can be placed onto the pulse in either the frequency or time domains: $BT = B/\delta f = T/\delta t$. Higher time-bandwidth product, corresponding to higher waveform complexity, is most easily attained for larger bandwidth, shorter duration pulses.

Fig. 3.4 illustrates an additional consequence of the diffraction effects sketched in Fig. 3.2. For these measurements short pulses centered around 1.56 μm were shaped using a pseudorandom phase-only mask with a series of abrupt 0–π phase transitions [44]. This results in generation of pseudonoise waveforms useful for studies of optical code-division multiple-access communications, in which different users are assigned different waveforms (codes) in order to share a common fiber optic transmission medium [13,45,46]. At each location in the spectrum corresponding to a phase transition, a deep notch is observed, with width approximately equal to the spectral resolution of the pulse shaper employed. These notches in the power spectrum arise because frequencies impinging on abrupt features are diffracted out of the main beam and are lost upon coupling into an output fiber following the pulse shaper. The simulated spectrum based on Eq. (3.4) is in excellent agreement with experiment, as seen in the figure. This shows that phase-to-amplitude conversion effects, as evident in Fig. 3.4, are a fundamental aspect of pulse shaping and should not be attributed simply to imperfections in the physical hardware.

A final point concerns causality in pulse shaping. In particular, a frequently asked question is how pulse shaping can create waveform content that appears not only after, but also prior to, the unshaped pulse — as evident from the pulse position modulation data of Fig. 2.2 (c), for example. The explanation is that the delay of the pulse in propagating through the pulse shaper is not taken into account in measurements such as those of Fig. 2.2. In these plots the zero of the time axis usually corresponds to the arrival time, at the location of the measurement apparatus, of a pulse transmitted through the pulse shaper in a quiescent state. Therefore, waveform content created prior to $t = 0$ does *not* correspond to light emerging from the pulse shaper before it went in; it simply corresponds to light emerging with delay slightly less than the large fixed delay of the quiescent pulse shaper. Pulse shaping action may be understood as causing light to travel through the apparatus with paths that are slightly shorter than (or slightly longer than) the path taken without pulse shaping action. The form of the coupled space–time field resulting from the analysis of [42] is consistent with this view.

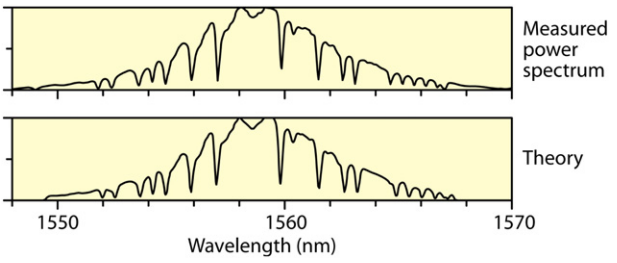

Fig. 3.4. Spectral dips arising from abrupt π phase shifts in pulse shaping mask. These results illustrate phase-to-amplitude conversion effects fundamentally arising from finite spectral resolution.

4. Programmable pulse shaping

The programmability feature of pulse shaping is very important, allowing a single apparatus to generate a wide range of waveforms for different experiments or applications. As mentioned earlier, programmable Fourier transform pulse shaping has employed a number of different programmable mask or spatial light modulator (SLM) technologies, including liquid crystal SLMs [4,23–25], acousto-optic modulators [26], and others. A detailed review of several useful SLM technologies is given in [4]; a more recent survey of programmable mask devices for Fourier pulse shaping is included in [9]. In this section we first review liquid crystal SLMs in the form that is now widely used for programmable pulse shaping. We then discuss liquid crystal on silicon (LCOS) SLMs, which have been considered for pulse shaping more recently, followed by pulse shaping using acousto-optic masks. Finally, we discuss an alternative programmable pulse shaping approach (not in the geometry of Fig. 2.1), termed an acousto-optic (programmable) dispersive filter (AOPDF). The AOPDF, which is based on co-propagating optical and acoustic waves, is now popular for use with amplified femtosecond systems.

4.1. Liquid crystal spatial light modulators

Fig. 4.1 depicts the basic layout of liquid crystal SLMs widely used for pulse shaping. This sketch shows a single layer device, which is useful, for example, for phase-only shaping [23,24]. As discussed below, double layer arrangements, which allow independent phase and amplitude shaping, are also common. The basic construction involves a thin region of a nematic liquid crystal material sandwiched between two glass plates. The nematic liquid crystal consists of long, thin, rod-like molecules, which lack translational order and which

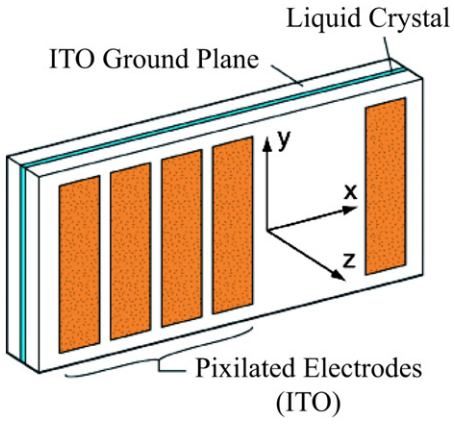

Fig. 4.1. Basic layout of liquid crystal spatial light modulator used for pulse shaping. Here a single layer SLM is pictured, which may be used for phase-only pulse shaping. SLMs in which two similar layers are aligned and bonded in a two layer configuration are in common use for phase and intensity pulse shaping.

may flow (similar to a liquid), but which maintain orientational order (similar to a crystalline solid). As depicted in Fig. 4.2(a), the liquid crystal cell is fabricated so that in the absence of an electric field, the molecules are aligned with their long axes along the y direction. This results in optical birefringence: light polarized along y (parallel to the long axes of the molecules) sees a larger refractive index than does light polarized along x (perpendicular to the long axes). When an electric field is applied, in the longitudinal (or z) direction, the liquid crystal molecules tilt along z, as depicted in Fig. 4.2(b), reducing the birefringence. As a result the phase of y-polarized light transmitted through the cell is changed via electric field control.

In order to apply the required electric field, the inside surface of each piece of glass is coated with a thin, transparent, electrically conducting film, such as indium tin oxide (ITO). One piece is patterned into a number of separate electrodes (or pixels) with the corresponding fan out for electrical connections; the conducting film on the other glass surface is unpatterned and serves as a ground plane. A typical device may be configured to comprise between 128 and 640 pixels, with center-to-center pixel spacings on the order of 100 μm, and gaps of only a few μm between adjacent pixels. Fig. 4.2(c) shows an example of the phase difference for y polarized light, relative to the phase at zero applied voltage, plotted as a function of applied voltage. Above some threshold voltage, the phase changes rapidly at first but eventually saturates as the molecules become aligned along the longitudinal direction. The maximum phase difference shown in Fig. 4.2(c) corresponds to the minimum birefringence. An attainable phase change of at least 2π is required for complete phase control, which (for a given zero-field birefringence) defines the minimum thickness of the liquid crystal layer. The phase vs. voltage response can be calibrated and stored in a look-up table. In one common method for calibration, one launches light polarized at 45° (relative to both the x and y axes), so that the polarization at the output is transformed due to the voltage-dependent birefringence. The fractional power transmission through a crossed-polarizer is given by

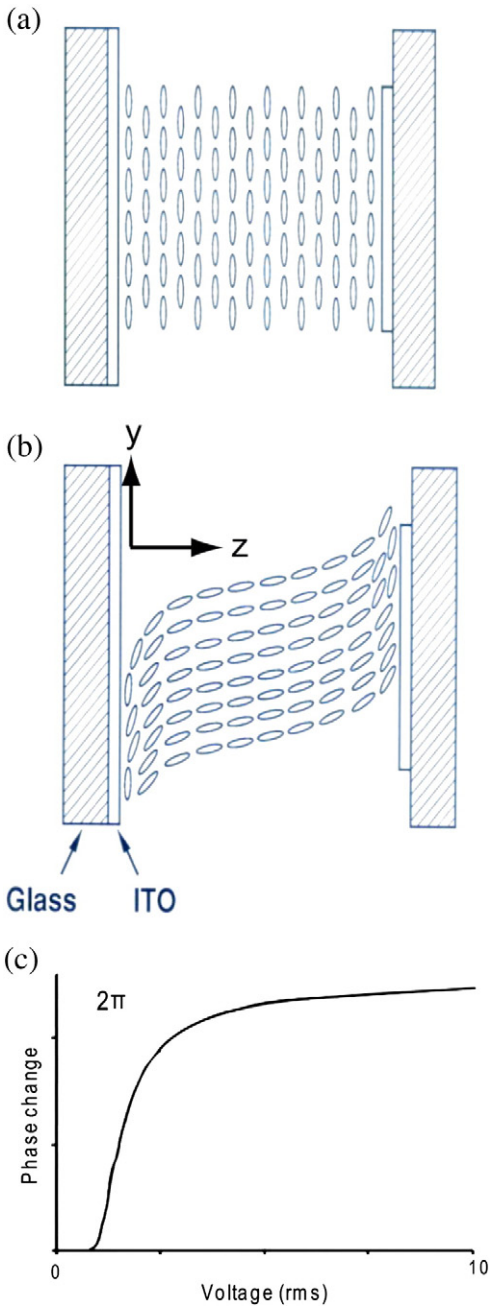

Fig. 4.2. Side view of a liquid crystal pixel in a configuration typical for pulse shaping. (a) No applied electric field. (b) Electric field applied in the longitudinal direction. (c) Representative plot of optical phase change as a function of applied voltage.

$$\frac{P_{out}}{P_{in}} = \sin^2\left[\frac{\Delta\phi(V)}{2}\right], \tag{4.1}$$

where $\Delta\phi(V)$ refers to the voltage-dependent birefringence. Thus, $\Delta\phi(V)$ can be extracted by measuring the power transmission as a function of applied voltage.

Generally a computer and multi-channel electronics are used to generate a user specified set of variable amplitude drive signals to achieve independent, gray-level control of all the modulator elements. It is worth noting that usually each drive signal actually consists of a variable amplitude bipolar square wave, typically at a few hundred Hz or above, rather than a variable amplitude direct current (dc) level. The use of an alternating current (ac) drive signal is required to prevent electromigration effects in the liquid crystal [47]. Otherwise the use of a square wave as opposed to a dc level does not change the operation of the modulator, since the rotation of the liquid crystal molecules depends only on the amplitude (not the sign) of the applied voltage. Assuming appropriately designed drive electronics, the masking function provided by a liquid crystal SLM may be held very nearly constant. Hence, when used with high repetition rate sources such as mode-locked lasers, successive pulses would be shaped identically. The speed with which the pulse shaper may be reprogrammed depends on the response time of the SLM, which is ultimately limited by the dynamics of the liquid crystal itself to milliseconds, and may be further limited by the control circuitry utilized.

The single layer SLM arrangements of Fig. 4.1 are primarily used for phase-only pulse shaping. Early versions of such SLMs were utilized in the experimental examples shown in Fig. 2.2(c,d). By using a 45° launch polarization, one can also use single layer devices for amplitude shaping, but only in situations where one does not care about accompanying phase changes. In order to achieve independent amplitude and phase control, a two layer SLM design is commonly used [25]. The layout is similar to that of Fig. 4.1, but with two such SLMs aligned and attached together back to back. The long axes of liquid crystal molecules in the first and second layers are aligned at 45° and −45° with respect to the x axis, respectively. When a voltage is applied to a pixel in one of the SLMs, the liquid crystal molecules in that pixel are rotated toward z, resulting in a phase modulation for the component of light parallel to the liquid crystal axis in that SLM. In the case where the input field and an output polarizer are both oriented parallel to y, the output field corresponding to some specific pixel is written [1,25]

$$E_{out} = E_{in}\exp\left[\frac{\Delta\phi_1(V_1) + \Delta\phi_2(V_2)}{2}\right]\cos\left[\frac{\Delta\phi_1(V_1) - \Delta\phi_2(V_2)}{2}\right] \tag{4.2}$$

where $\Delta\phi_i(V_i)$ is the voltage dependent birefringence of the ith layer. The transmitted power depends on the difference in the birefringences of the two layers, while the phase imparted depends on the average of the two birefringences. Hence $\Delta\phi_1$ and $\Delta\phi_2$ can be chosen to control amplitude and phase independently.

Dual layer liquid crystal SLMs have also been used for polarization pulse shaping [48]. In this case the output polarizer is not used. This configuration permits independent phase shaping of two orthogonal polarization components, which means that the frequency-dependent polarization is confined to a great circle on the Poincare sphere. More recently independent phase and amplitude shaping of two orthogonal polarization components has been achieved [49,50]. In these near-common path interferometer schemes, orthogonal polarizations are mapped to different regions of the same spatial light modulator. With careful balancing of the delays in the separate paths, realization of general frequency-dependent polarizations states becomes possible. Another approach uses a concatenation of four or more liquid crystal layers and fixed polarization optics to achieve full spectral phase, amplitude, and polarization shaping in fully common path configuration [51]. The liquid crystal arrangement utilized in this latter scheme is closely related to a four layer liquid crystal geometry used for compensation of polarization mode dispersion in optical fibers [52,53], described in Section 5.2.

4.1.1. Large pixel count SLMs

The number of control pixels available in an SLM is limited by the interconnect problem: it is difficult to bring more than a few hundred separate electrical leads into the vicinity of the optically active region. An increased number of control pixels is useful in order to engineer greater complexity into shaped waveforms or, in the case of two-dimensional SLM formats, to support novel functionalities.

Particularly interesting in this context are devices based on liquid crystal on silicon (LCoS) [54–56], a relatively new technology aimed primarily at microdisplay applications. LCoS SLMs are reflective devices in which a single liquid crystal layer is placed directly on a silicon chip which applies drive signals to a pixellated electrode array which is fabricated onto the silicon itself. A mirror is deposited on top of the silicon, above which are placed the thin liquid crystal layer and a cover glass with ITO ground plane. A primary benefit of this approach is that because the pixels are directly fabricated on the driving circuit, the pixel count can be very large. Both one dimensional (1D) LCoS arrays, with pixel count $>10^4$ [57], and two dimensional (2D) arrays, with pixel count $>10^6$ [58], have been demonstrated in pulse shaping experiments.

In conjunction with the increased available pixel counts, individual pixels of an LCoS device are typically much smaller than for a conventional liquid crystal SLM. Fig. 4.3(a–c) illustrates the geometry of conventional, 1D LCoS, and 2D LCoS SLMs, respectively. For a well designed pulse shaper, the pixel size (e.g., 100 μm) of a typical conventional liquid crystal SLM would be comparable to spot size of any single frequency at the Fourier plane ($2w_o$ in Eq. (3.4)). However, the pixel sizes for the 1D and 2D LCoS devices reported in references [57] and [58] were 1.6 μm and 8 μm, respectively. Now any single frequency will usually have a spot size much larger than an individual pixel. Accordingly, groups of pixels are used as "superpixels" to control individual frequency components. Note also that for the smallest pixel sizes, the inherent spatial resolution of the SLM itself may also be significantly coarser than the pixel sizel, depending on the spread of electric fringing fields.

Because LCoS only provides a single liquid crystal layer, a new approach is needed to achieve simultaneous, independent amplitude and phase control. Fortunately, the over-sampling evident in Fig. 4.3 (b,c) permits the formation of diffractive patterns by applying different drive levels to the various pixels making up each superpixel. This concept is illustrated in Fig. 4.4, which depicts the phase programmed vs. position in a 1D geometry. Three superpixels are included in the illustration. According to [57], the phase vs. position (x) is taken to have the form of a sinusoidal grating,

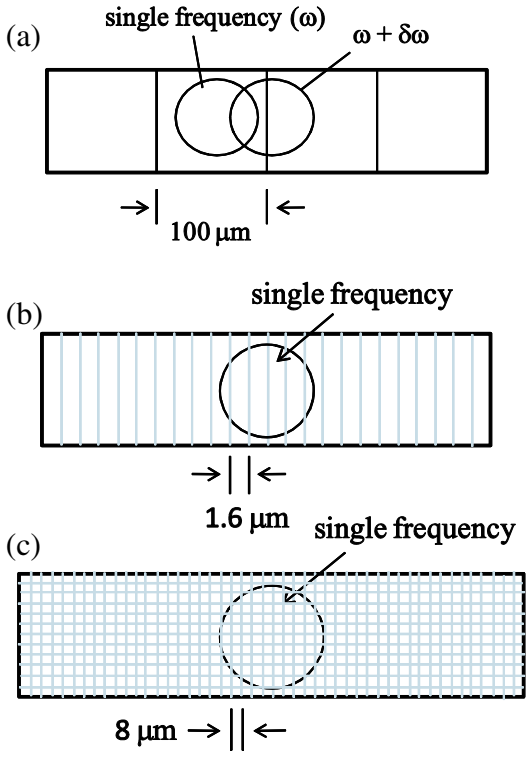

Fig. 4.3. Schematic illustration of geometries for (a) conventional, (b) one dimensional LCoS, and (c) two dimensional LCoS spatial light modulators. The typical beam size of a single optical frequency component in a pulse shaping scenario is also shown.

$$M(x) = \exp\left[i\,\Delta(x)\sin\left(\frac{2\pi x}{\Lambda}\right) + i\,\Phi(x)\right] \tag{4.3}$$

When the grating period Λ is sufficiently small compared to w_o, light is diffracted into discrete orders with amplitudes determined by the phase excursion of the grating, 2Δ. This provides a mechanism for coupling power out of the reflected zero-order beam and hence controlling its amplitude. On the other hand, the phase of the reflected zero-order beam is governed by the average applied phase $\Phi(x)$. Thus, independent phase and amplitude control is achieved.

Experiments testing reflective 2D LCoS SLMs for pulse shaping have investigated both zero-order and first-order diffraction geometries [58]. It was reported that the zero-order geometry resulted in the lower insertion loss, while the first-order geometry gave the best extinction ratio. Similar diffractive schemes were also utilized in earlier pulse shaping experiments employing 2D liquid crystal SLMs that were optically addressed [59]. The 2D SLM format makes possible a number of interesting new functionalities. These include: generation of a set of independently shaped waveforms separated either in space

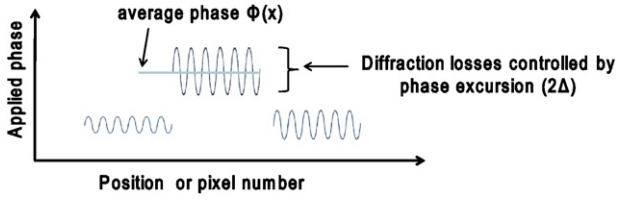

Fig. 4.4. Approach for pulse shaping control using phase-only LCoS SLMs. The oversampling provided by the small pixel size allows for formation of diffractive structures, which enable independent phase and intensity control.

or in wave vector [59–61], with application for example to multi-dimensional nonlinear optical spectroscopy [62]; rapid waveform update by scanning the beam across different rows of the SLM [63]; and realization of significantly increased waveform complexity in conjunction with a novel, two dimensional spectral dispersion geometry [64,65].

Finally, pulse shapers incorporating 2D phase-only SLMs have been adapted to realize commercial wavelength selective switches that are deployed in optical communications networks [66]. Here the SLM deflects input light by different angles in the direction perpendicular to the spectral dispersion direction, allowing coupling into different output fibers under programmatic control. As usual in pulse shaping, different wavelengths may be switched independently, and arbitrary attenuation for each wavelength may also be achieved. Although closely related to pulse shapers, in the lightwave industry such modules have come to be known by terms such as dynamic wavelength processors. Recently it was recognized that spectral phase may be controlled simultaneously by appropriately varying the phase in the spectral dispersion direction. This enables simultaneous wavelength selective switching and chromatic dispersion trimming [67], a functionality that has also been introduced commercially. Further discussion of pulse shaping applications to optical communications is given in Section 5.2.

4.2. Acousto-optic pulse shapers

Acousto-optic (AO) modulators have also been used for programmable Fourier transform pulse shaping [26]. In an AO modulator, a radio-frequency electrical signal drives a piezoelectric transducer, which launches a traveling acoustic wave into an appropriate medium. Modulator action is based on diffraction of the light beam from refractive index changes induced by the traveling acoustic wave. The diffracted beam is shifted in frequency by an amount equal to the electrical drive frequency (typically in the one hundred MHz range), ideally with an amplitude and phase that directly reflect the amplitude and phase of the RF drive. As illustrated in Fig. 4.5, the pulse shaping setup is similar to that of Fig. 2.1, but with the optical elements displaced to account for the beam deflection that accompanies AO modulation. In the case of a modulated RF drive, the spatial profile of the acoustic wave across the aperture of the device is a scaled and delayed version of the temporal drive signal. Accordingly, by using an electronic arbitrary waveform generator (which in this frequency range is a mature commercial technology) to drive the AO modulator, the acoustic profile can be controlled, and programmable pulse shaping achieved (though care may be needed to account for acoustic attenuation and nonlinearities).

Because pulse shaping occurs via diffraction from a traveling acoustic wave, the mask inherently has a traveling wave nature. In general, this is not suitable for pulse shaping applications involving high repetition rate pulse trains from typical mode-locked laser sources, because fundamentally the mask, and hence the shaped pulses, vary in time. (For some special applications, however, the time variation can be cleverly exploited, e.g., [68]). However, there is no problem for applications involving amplified femtosecond systems. The reprogramming time for an AO modulator is limited by the acoustic travel time across the device aperture. Typically this is on the order of tens of microseconds, which is fast enough to allow the pulse shaping mask to be refreshed, or updated, on a shot-by-shot basis for KHz repetition rate systems.

It should be noted that AO modulators produce a mask with continuous spatial modulation, which is in contrast to the pixelated nature of conventional liquid crystal SLMs. Time-bandwidth products of several hundred, comparable to that available with liquid crystal technologies, have been demonstrated. AO based pulse shapers have been demonstrated over a wavelength range from 260 nm [69] to 5 μm [70], which supports spectroscopy applications in the ultraviolet and mid-infrared. (In contrast, liquid crystal SLMs usually have transmission limited to the visible and near-infrared bands.)

4.3. Acousto-optic programmable dispersive filters

Acousto-optic interactions also enable a quite different type of programmable pulse shaper [71,72], shown schematically (in somewhat simplified form) in Fig. 4.6. The input optical field is launched with polarization along one of the principle axes of a birefringent photoelastic crystal. In the absence of any interaction, light is extinguished at the output by a crossed polarizer. An acoustic wave launched collinearly with the optical wave produces an additional, periodic, stress-induced birefringence that couples light from the input polarization into the orthogonal polarization state (which is transmitted by the polarizer). When the acoustic wave is driven by a single electrical tone, the result is an optical bandpass filter, with center frequency determined by the phase matching condition that the acoustic wavelength match the birefringent beat length. This enables tuning of the optical bandpass frequency by varying the electrical (hence acoustic) frequency. In this mode of operation, the device is known as an acousto-optic tunable filter [73,74].

For pulse shaping applications the optical input is a pulse, and the acoustic wave is time-varying, corresponding to a superposition of different acoustic frequencies [71,72,75]. In this mode the optical pulse shape at the output can be shown [1] to be, approximately, a scaled version of the acoustic spatial profile along the length of the device. Because the acoustic waveform may be controlled in turn by connecting a radio-frequency arbitrary waveform generator to the acoustic transducer, programmability is easily achieved. In this pulse shaping mode of operation, the device has been termed an acousto-optic programmable dispersive filter (AOPDF) [71,72]. As in the

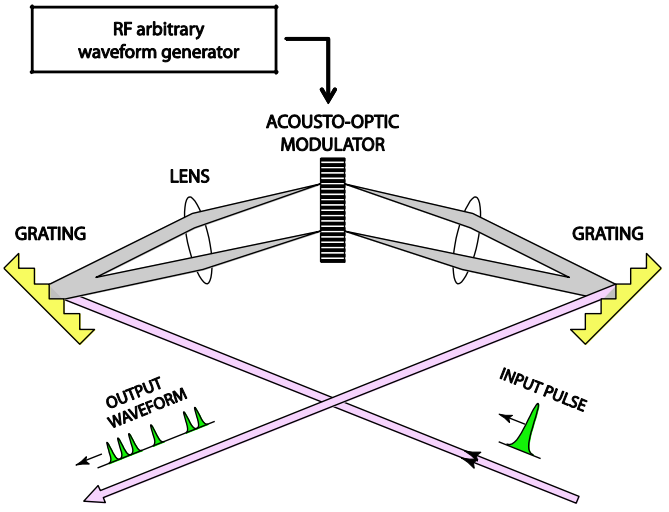

Fig. 4.5. Schematic setup for Fourier transform pulse shaping using acousto-optic modulator.

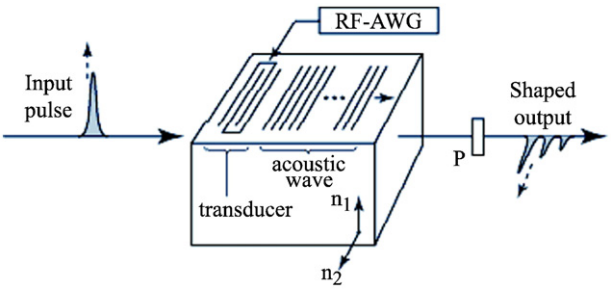

Fig. 4.6. Geometry of an acousto-optic programmable dispersive filter.

acousto-optic pulse shapers of Section 4.2, the traveling wave nature of the acoustic signal means that the pulse shaping function varies in time. Consequently AOPDFs are useful primarily as a compact, in-line pulse shaping technology for amplified femtosecond systems. Because AOPDFs are constructed from materials similar to those used for the acousto-optic pulse shapers of the previous section, there is potential for devices spanning an analogously broad wavelength range. For example, an AOPDF operating down to 250 nm in the ultraviolet was recently reported [76].

To illustrate, we consider typical numbers. Reference [72] reported an AOPDF constructed from a 2.5 cm long TeO_2 crystal, which has a birefringent index difference of 0.04 and an acoustic velocity of 10^5 cm/s. The device was designed for 52.5 MHz acoustic center frequency, with 20 MHz acoustic bandwidth. This translates into phase matched operation over 150 THz optical bandwidth around a center frequency of 375 THz (800 nm wavelength). The large bandwidth implies capability to manipulate few cycle pulses. The acoustic transit time defines the maximum rate at which the pulse shaping function can be refreshed or updated. In this example, the acoustic transit time is 25 μs, fast enough for pulse-by-pulse update of KHz class femtosecond amplifier systems. The maximum time aperture over which pulse shaping may be achieved is determined by the different optical transit times for waves polarized along fast and slow birefringent axes. In this example the difference in transit times (hence the pulse shaping time aperture) is 3.3 ps, resulting in a time-bandwidth product up to several hundred. This is achieved only when using very short pulses, for which it is essential to compensate the group velocity dispersion of the AOPDF material. This may be achieved either by programming the AOPDF itself or though external means.

5. Selected applications

Programmable pulse shaping has served as an enabling technology for a broad range of applications, both in ultrafast science and technology. Examples include coherent manipulation of light–matter interactions, spectrally (hence chemically) selective nonlinear microscopy, phase compensation and pulse compression, single cycle pulse generation, lightwave communications, and radio-frequency photonics. In this section I principally discuss some examples in the areas of coherent control and lightwave communications. In a later section (Section 7), I present examples in radio-frequency photonics. Compensation of phase is a very important use of pulse shaping, which occurs in many contexts. These range from dispersion compensation for transmission of fast optical signals over fiber cables as well as for wireless transmission of ultrawideband radio-frequency electrical pulses over broadband antennas, to single cycle pulse generation and optimization of pulses from chirped pulse amplifier systems.

Before going into specific examples, it is worth commenting on two contrasting control strategies for programmable pulse shaping, namely, open loop control and feedback (adaptive) control, both of which are depicted in Fig. 5.1. In the open loop configuration, the desired output waveform is specified by the user, and reasonable knowledge of the input pulse is also usually available. Therefore, the desired transfer function is known, and one simply programs the pulse shaping SLM to provide this transfer function. If there is additional linear distortion present between the input and output (e.g., phase aberration in a femtosecond amplifier, not shown), the pulse shaper can be programmed so that its transfer function also includes precompensation for such distortion. This open loop strategy requires precise calibration of the SLM.

The ability to program a pulse shaper under computer control leads also to an alternative adaptive control strategy [77–79]. In these experiments one usually starts with a random spectral pattern programmed into the pulse shaper, which is updated iteratively according to a stochastic optimization algorithm based on the difference between a desired and measured experimental output. In this scheme there is no need to explicitly program the pulse shaper. The adaptive control scheme is less intuitive but is often viewed as especially suitable for optimization of strongly nonlinear processes or for manipulation of quantum mechanical motions in systems, such as molecules, where knowledge of the Hamiltonian may be insufficiently accurate [80]. In such cases the adaptive control approach can be used to search for the laser waveform which gives the best experimental result, such as optimizing the yield of a particular photochemical product [81]. In such cases the adaptive control approach can be used to search for the laser waveform which gives the best experimental result, as judged according to a user-defined metric. Examples of experiments in which this adaptive control strategy has been successfully applied include: laser controlled chemistry (e.g., control of reaction products in laser photo-dissociation reactions) [81–84], selective enhancement of high harmonic (soft X-ray) radiation from atoms driven by strong laser fields [85], nonlinear pulse propagation in fibers [86], manipulation of energy flow in light harvesting molecules [87], and spatially selective excitation of plasmons in subwavelength metallic nanostructures [88,89].

5.1. Open loop coherent control for spectroscopy, microscopy, and other applications

Here we will discuss a few examples of coherent control involving the open loop control strategy, first explaining examples in spectroscopy, then briefly discussing how similar principles find some applications in signal processing and in ultrashort pulse measurement.

In our first example, we consider impulsive stimulated Raman scattering (ISRS) [90,91] experiments, in which an ultrashort pulse excites coherent vibrational motion in a transparent, Raman active material. In one popular experimental geometry, a noncollinear pair of pump pulses cross at an angle and excite a vibrational standing wave that acts as a time-varying transient refractive index grating. By measuring diffraction of a short pulse as a function of probe pulse delay, one can monitor the time dependence of the vibrational coherence. A distinctive feature of ISRS is that both pump and probe pulses should have durations short compared to the vibrational period, which means that their bandwidths are larger than the vibrational frequency. This is in contrast to conventional Raman scattering performed with nondegenerate, narrow band fields.

Fig. 5.2(a) shows ISRS data from a molecular crystal sample [91–93]. The signal consists of a sharp peak at zero delay, arising from the essentially instantaneous nonlinearity associated with distortion of the electronic wave function, followed by a long tail corresponding to optical phonons excited through ISRS. A few points are of note. First, the intensity of the ISRS signal is weak compared to that arising from the electronic scattering peak. Second, the ISRS diffraction intensity presents an irregular pattern that is caused by beating among several simultaneously excited phonon modes. Fig. 5.2(b) shows a Fourier transform of the scattering data (with the electronic peak removed). The result consists of a complicated series of lines at frequencies corresponding to sum and difference frequencies of vibrational modes. Although such data clearly demonstrate the ability to excite and monitor coherent vibrational motion, they also reveal some limitations: (1) the vibrational response is small, at least in comparison with the electronic scattering peak which provides an internal intensity calibration; and (2) there is lack of mode selectivity — a short pulse excites any Raman-active mode whose vibrational frequency falls within the instrumental response.

These issues may be addressed by driving the system with a train of pulses [92,93]. In particular, when the vibrational frequency of a particular mode is matched to the repetition rate of the pulse train, that mode is selectively amplified. This is demonstrated by the data of Fig. 5.2(c,d). Fig. 5.2(c) shows the intensity profile of an approximately 2.4 THz pump-pulse train, generated via periodic spectral

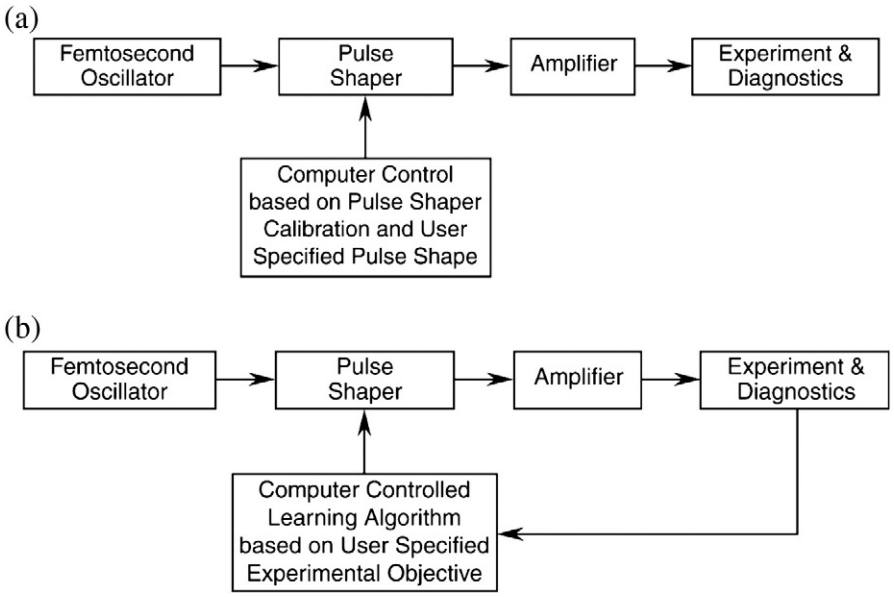

Fig. 5.1. Control strategies for programmable pulse shaping. (a) Open-loop control. (b) Feedback or adaptive control.

phase filtering in a pulse shaper and timed to match the period of a specific vibrational mode. Fig. 5.2(d) shows the resulting ISRS data, read out as usual using a single probe pulse. Initially the signal is dominated by the crystal's electronic response to each of the pulses in the sequence. However, the vibrational signal builds up as the pulse train progresses. By the end of the pulse train, the ISRS signal is approximately as intense as the strongest electronic scattering peak. Furthermore, in contrast to the single pulse experiments, the ISRS signal after the pulse train has ended appears to be oscillatory at a single frequency, and the dephasing of the excited mode is now clearly discernible. These results comprised a simple, early example of the use of shaped femtosecond waveforms for control over molecular motion.

Related coherent control methods have become popular to enhance nonlinear optical spectroscopy and microscopy, e.g., in order to emphasize a spectral feature of interest. A recent review of this field may be found in [10]. As one example, pulse shaping enables single beam, chemically selective nonlinear spectroscopy via coherent anti-Stokes Raman scattering (CARS) [94]. As illustrated by Fig. 5.3 [10], femtosecond pulses are shaped and then focused tightly into the

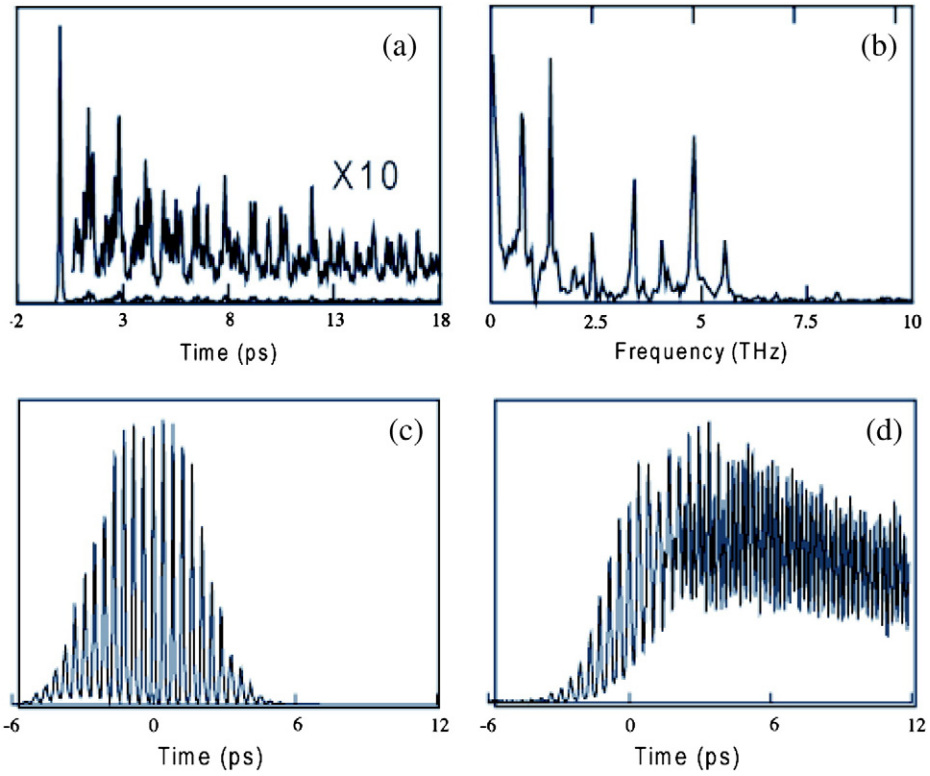

Fig. 5.2. ISRS data from a molecular crystal sample. (a) ISRS signal using unshaped pulses, and (b) resulting Fourier transform. (c) Shaped pulse train used for multiple pulse ISRS excitation, and (d) resulting ISRS signal.

sample of interest. The nonlinear output signal is detected, and the sample is scanned to form an image. For Raman processes the amplitude q of a vibrational resonance (with frequency Ω_{vib}) impulsively stimulated by a shaped light field is given by

$$q \sim \int d\omega E(\omega) E^*(\omega - \Omega_{vib}) = \int d\omega \left| E(\omega) | E(\omega - \Omega_{vib}) \right| e^{j[\psi(\omega) - \psi(\omega - \Omega_{vib})]} \quad (5.1)$$

where $\psi(\omega)$ is the spectral phase. Hence, a sinusoidal spectral phase function (or other periodic phase function) with period Ω_{vib} generates the same vibrational amplitude as a bandwidth-limited pulse. This property is closely related to the multiple pulse ISRS experiments described above and provides a mechanism for mode selectivity, which otherwise would be absent in experiments with broad bandwidth, femtosecond pulses. An additional pulse shaping trick is to block the short wavelength end of the excitation signal to support background-free detection of the CARS signal, which is up-shifted from the input spectrum by the vibrational frequency. Key advantages motivating interest in such approaches include the simple in-line geometry and the possibility to use pulse shaping simultaneously for programmable dispersion control and to reduce the nonresonant background.

Fig. 5.4(a) illustrates a concept for quantum control of two photon absorption (TPA) in cesium vapor [95]. Unlike the previous example, which may be understood classically, this concept explicitly depends on discrete energy levels and is therefore fundamentally quantum mechanical in nature. The central point is that when a broadband signal with complex spectrum $E(\omega)$, centered around half of the two photon transition frequency Ω_{TPA}, excites a two photon transition without intermediate levels, different pairs of field components can mix in the TPA process, subject to the condition that the sum of their frequencies equals the two photon frequency. In the weak field limit, the wave function amplitude c_2 of the upper level state excited by TPA is given by

$$c_2 \sim \int d\omega E(\omega) E(\Omega_{TPA} - \omega) = \int d\omega \left| E(\omega) E(\Omega_{TPA} - \omega) \right| e^{j[\psi(\omega) + \psi(\Omega_{TPA} - \omega)]} \quad (5.2)$$

Hence spectral phase shaping can be used to manipulate the interference between two photon excitation pathways, leading to coherent control of the two photon excitation probability.

Fig. 5.5 shows an example of experimental results from [95]. Here a sinusoidal or cosinusoidal spectral phase modulation was applied onto the excitation pulse, and the strength of the resulting TPA was determined by monitoring fluorescence. For cosinusoidal spectral phase, $\psi(\omega) = \alpha \cos(\omega - (1/2)\Omega_{TPA})$, the two photon yield drops off quickly and then oscillates as the amplitude (α) of phase modulation increases. For certain values of α, the TPA is extinguished; for these pulses there is complete destructive interference between the various excitation pathways. On the other hand, for sinusoidal spectral phase, $\psi(\omega) = \alpha \sin(\omega - (1/2)\Omega_{TPA})$, the TPA falls off only slowly. For these waveforms corresponding to antisymmetric spectral phase, the phase completely drops out from Eq. (5.1). Hence all excitation pathways interfere constructively, and ideally one obtains the same two photon

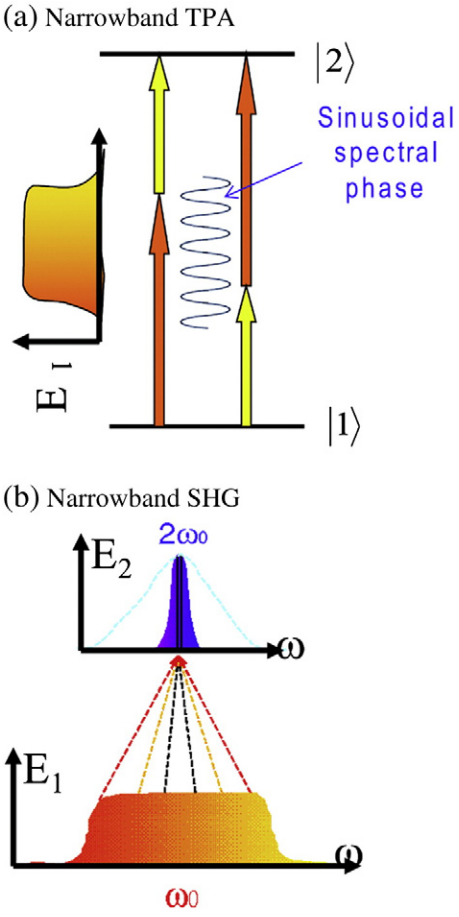

Fig. 5.4. (a) Conceptual view of two photon absorption to a discrete level with broadband shaped pulses. (b) Conceptual view of second harmonic generation with broadband pulses. In the case of narrow phase matching bandwidth, the upconverted spectrum is narrow compared to the spectrum of the nonlinear polarization (dashed blue line).

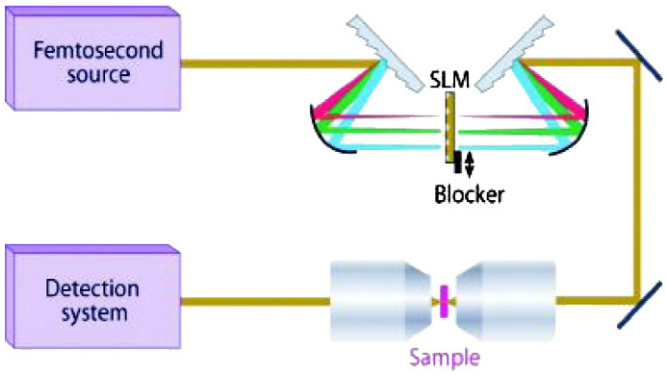

Fig. 5.3. Schematic representation for single beam, shaped pulse, coherent anti-Stokes Raman spectroscopy (CARS). Reproduced from [10] with permission of ANNUAL REVIEWS, INC. (© 2009 ANNUAL REVIEWS, INC.).

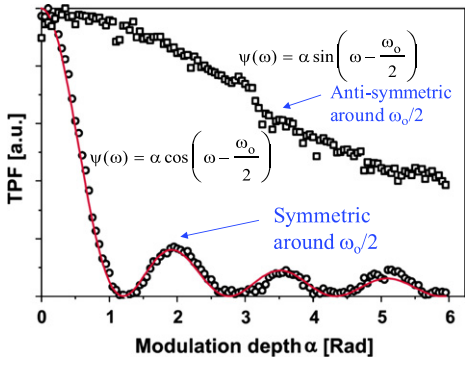

Fig. 5.5. Data showing coherent control of two photon absorption to a discrete level via periodic spectral phase modulation. The two photon yields for cosinusoidal (symmetric) and sinusoidal (antisymmetric) spectral phase modulation differ dramatically. Adapted from [95], by permission from Macmillan Publishers Ltd: Nature, © 1998.

yield as for the optimum, bandwidth-limited excitation. The slow roll-off with increasing α is attributed only to finite spectral resolution or nonidealities of the pulse shaper. These results convincingly demonstrate the ability to manipulate interference between a multiplicity of two photon absorption pathways for creation of user selectable "dark" or "light " pulses.

Similar ideas apply to coherent control of classical second harmonic generation (SHG), with applications both to novel forms of optical communications and pulse characterization. Fig. 5.4(b) illustrates the concept for the case of narrowband SHG, in which the phase matching bandwidth is much narrower than the spectrum of the exciting pulse [96,97]. As in TPA, spectral components of the input electric field (assumed to be centered at frequency ω_o) sum in pairs to yield the second harmonic field centered at frequency $2\omega_o$ (which is assumed to be phase matched). For this narrowband phase matching case, the amplitude of the generated second harmonic field is given by

$$e_{2\omega_o} \sim \int d\omega E(\omega)E(2\omega_o-\omega) = \int d\omega \left|E(\omega)E(2\omega_o-\omega)\right| e^{j[\psi(\omega) + \psi(2\omega_o-\omega)]} \tag{5.3}$$

which is exactly analogous to Eq. (5.2) for TPA. Therefore, the SHG yield depends on the spectral phase correlations of shaped input field. This dependency has been exploited for decoding of spectral phase codes applied to short pulse signals in experimental studies of optical code-division multiple-access (OCDMA) lightwave communications. In particular, it was shown that one can use the narrowband SHG process of Eq. (5.3) to look for matches between a pair of phase codes, one applied onto the short wavelength side of the optical spectrum and the other applied onto the long wavelength side [96,97]. For appropriately selected code pairs, the coherent interference process yields approximately 30 dB contrast in generated second harmonic power for matched (i.e., phase is antisymmetric about ω_o) vs. unmatched code pairs. Four-user, 10 Gb/s communications experiments using such SHG-based decoding are reviewed in [46]. A key advantage of the SHG-based approach for nonlinear processing is that by taking advantage of highly efficient, periodically-poled lithium niobate waveguide technology [98,99], individual bits can be decoded with low error rate and high speed at energies corresponding to only ~50 fJ per bit. Such lower power operation, which is unusual within the scope of nonresonant nonlinear optics, is essential for compatibility with high rate, multi-user lightwave systems requirements.

Related ideas form the basis for a technique for characterization of ultrashort light pulses that has been termed the multiphoton intrapulse interference phase scan method (MIIPS) [100,101]. In particular, MIIPS makes use of the relationship between spectral phase modulation of an input pulse and the second harmonic spectrum resulting from broadband SHG experiments (i.e., with broad phase matching bandwidth). Similar to Eq. (5.3), the second harmonic spectrum is given by

$$\left|E_{SHG}(2\omega)\right|^2 \sim \int d\omega \left|E(\omega+\omega')E(\omega-\omega')\right| e^{j\left[\psi(\omega+\omega') + \psi(\omega-\omega')\right]} \tag{5.4}$$

where ω is the frequency variable in the fundamental frequency band. Peaks in the SHG spectrum are expected for frequencies 2ω such that the spectral phase of the pulse is antisymmetric about ω. Approximately, we may say that peaks occur for frequencies where the second derivative of the spectral phase $\psi''(\omega)$ vanishes. In MIIPS this idea is exploited in a simple setup using a pulse shaper, second harmonic crystal, and a spectrometer. The pulse shaper is used to intentionally add a known spectral phase $\psi_{MIIPS}(\omega)$, so that the total phase is $\psi(\omega) = \psi_{pulse}(\omega) + \psi_{MIIPS}(\omega)$, where $\psi_{pulse}(\omega)$ is the spectral phase of the pulse without additional phase applied by the shaper. Although various spectral phase functions are possible, a common choice is a sinusoid, $\psi_{MIIPS}(\omega, \delta) = \alpha \sin(\gamma\omega + \delta)$. A series of SHG spectra are recorded for various values of the δ parameter, forming a two dimensional plot. Because peaks occur approximately when the condition $\psi''_{pulse}(\omega) + \psi''_{MIIPS}(\omega, \delta) = 0$ is satisfied, and because $\psi_{MIIPS}(\omega, \delta)$ is known, this provides an estimate of $\psi''_{pulse}(\omega)$, which can be integrated to obtain an estimate of $\psi_{pulse}(\omega)$. The pulse shaper may then be programmed to compensate the estimated spectral phase, resulting in a pulse compressed closer to the bandwidth limit. This process is iterated on the compressed pulse, resulting in measurements that are increasingly accurate and pulses that are increasingly close to the bandwidth limit. Shaper-assisted pulse characterization methods such as MIIPS are increasingly applied in systems in which a pulse shaper will be used anyway, either for pulse compression purposes or for more general waveform generation. Some recent examples in which MIIPS is used to guide pulse compression of few cycle pulses may be found in [102,103].

5.2. Lightwave communications

Pulse shaping ideas also have significant applications for lightwave communications. As sketched in Fig. 5.6, we may generalize our picture to consider various forms of broadband inputs, including not only ultrashort pulses, but also continuous-wave lasers that are modulated with data and multiple wavelength sources. For example, in wavelength-division multiplexed (WDM) communications, the input consists of multiple, independently modulated laser sources at different center frequencies. Because the various sources are usually mutually incoherent, manipulation is performed on a wavelength-by-wavelength basis, but with no concern for phase between channels. This is in sharp contrast to shaping of ultrashort pulses, where phase coherence across the entire spectrum is an essential ingredient. Pulse shaping arrangements have been most applied for manipulating the

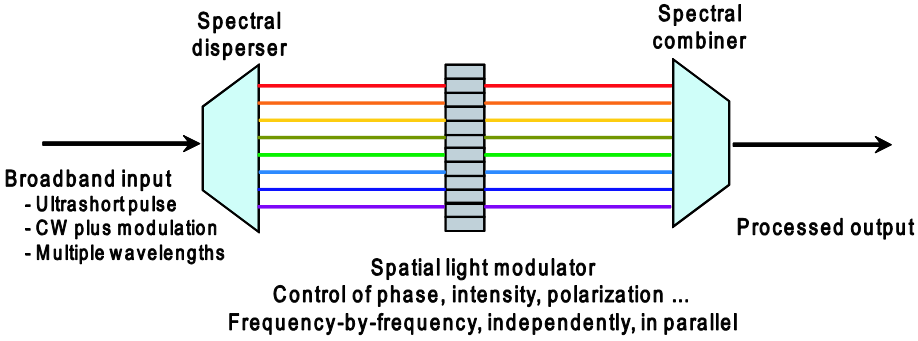

Fig. 5.6. Generalized view of pulse shaping, including not only ultrashort pulses, but also continuous-wave lasers that are modulated with data and multiple wavelength sources. In the wavelength-division multiplexed optical communications community, signal manipulation based on generalized pulse shaping geometries is often referred to by terms such as dynamic wavelength processors.

power spectrum of WDM signals, e.g., to correct for the effect of wavelength-dependent optical amplification or to achieve wavelength-selective optical switching (where a switch handling multiple wavelengths may be programmed to impose different, independent switching operations on different wavelengths). Recently, increasing attention is being given to manipulation of spectral phase within individual wavelength channels as well. Within the lighwave communications area, pulse shaping arrangements and their adaptations are often now referred to by terms such as "dynamic wavelength processors" and "dynamic spectral equalizers." Although not shown in the figure, for applications such as wavelength selective switching, the apparatus may be modified to encompass multiple input and output fibers. A common theme is that in all cases, one manipulates light frequency by frequency, independently and in parallel. One contrast between pulse shaping applications in lightwave communications and in ultrafast science centers around polarization: while the input polarization is usually well known and stable in ultrafast science settings, the polarization of light transmitted through fiber cables is usually unknown and at least slowly time-varying. For this reason lightwave modules inspired by pulse shaping may be constructed using a polarization diversity scheme, in which the input light is split into two orthogonal polarization components which are manipulated separately and then recombined to form the output signal.

Fig. 5.7 illustrates spectral gain equalization using a pulse shaper actuated by a MEMS micro-etalon structure that acts as an intensity spatial light modulator [104]. In this experiment 36 WDM channels spread over 30 nm in the lightwave C band were amplified in an erbium doped fiber amplifier (EDFA). As evident from Fig. 5.7(a), the nonuniformity of the EDFA gain results in 7.1 dB power variation across the optical spectrum, which can unacceptably impact signal-to-noise margin in system operation. Fig. 5.7(b) shows the results obtained with the pulse shaper programmed to equalize the power spectrum. A much smaller power variation of only 0.7 dB across the spectrum is observed.

Wavelength-selective switches and wavelength-selective add-drop multiplexers extend wavelength-by-wavelength intensity control to multiple input or output fiber ports. Fig. 5.8(a) depicts an example of an early, relatively simple generalized pulse shaping setup with two input ports and two output ports [105]. An array of MEMS tilt mirrors are used to control which input port is connected to which output port. The key point is that because the wavelength channels are separated, with each channel focused onto its own tilt mirror, the input–output connection can be programmed independently for each of the wavelengths. Fig. 5.8(b) shows an example of wavelength-by-wavelength switching action, in which several of the input wavelengths have been dropped. An earlier version of wavelength-selective switching with two output fibers, based on a liquid crystal spatial light modulator, was reported in [106]. More recent examples of wavelength selective switches, which use 2D liquid crystal SLMs to achieve switching between larger number of ports while also providing intrachannel spectral phase control, were discussed briefly in Section 4.1.1 [66,67].

In the following we concentrate on spectral phase control. This can be used for compensation of chromatic dispersion, which broadens the durations of signals sent through fiber optic links. Unless compensated, such broadening leads to intersymbol interference which limits the bit rates of high-speed optical fiber communication links. Physically, chromatic dispersion represents frequency dependent group velocity and frequency dependent delay. As expressed in Eq. (2.1), the frequency dependent delay $\tau(\omega)$ is fundamentally related to the derivative of the frequency dependent phase $\psi(\omega)$. Hence, one can compensate for the effect of dispersion by programming a pulse shaper

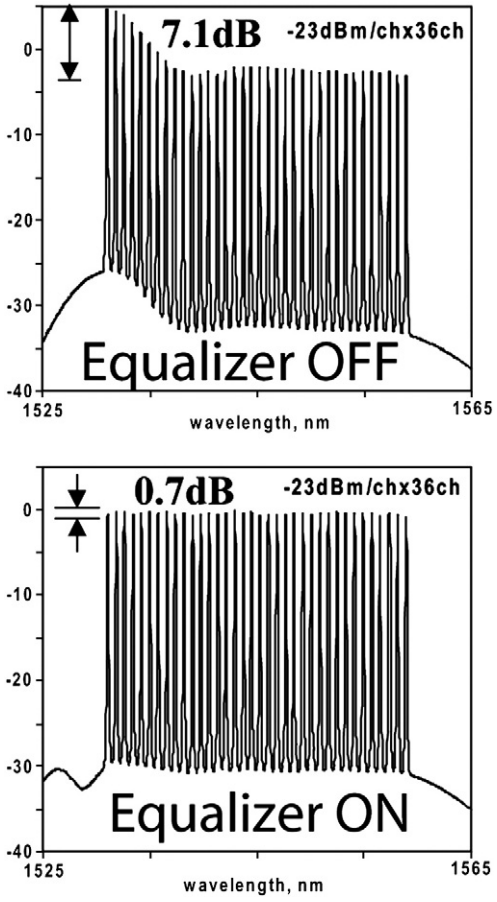

Fig. 5.7. Spectral gain equalization using a pulse shaper actuated by a MEMS structure that acts as an intensity spatial light modulator. Reprinted with permission from [104] (© 2004 IEEE).

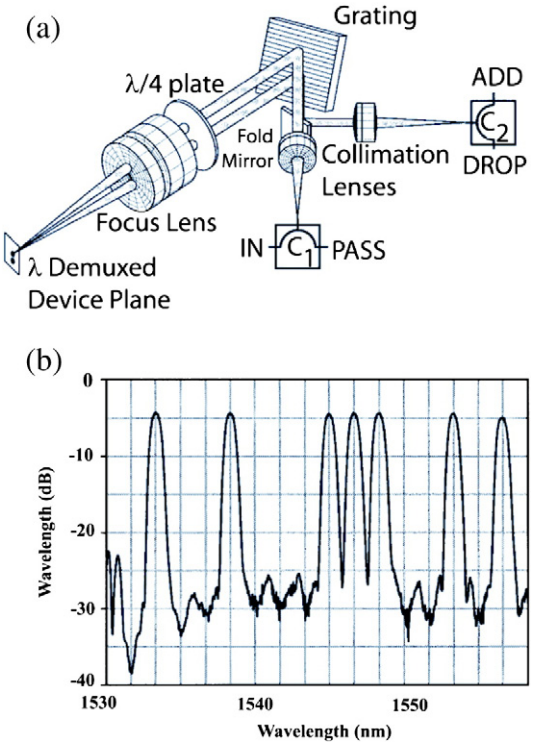

Fig. 5.8. (a) Example of generalized pulse shaping setup with two input and two output ports, and (b) data representing wavelength-by-wavelength optical switching action using this setup. Reprinted with permission from [105] (© 1999 IEEE).

to impose a spectral phase function equal and opposite to that specified in Eq. (2.1).

A block diagram of experiments demonstrating such dispersion compensation is shown in Fig. 5.9. Here a programmable pulse shaper was used to complement fiber dispersion compensation techniques in propagating sub-500 fs pulses over optical fiber links ranging from 3 km in early experiments to 50 km most recently [107–109]. In all cases the link consisted of a length of standard single-mode fiber (SMF) concatenated to an approximately matching length of dispersion compensating fiber (DCF). Since SMF and DCF have dispersion with opposite signs at the operating wavelength, the fiber lengths can be adjusted to cancel all of the lowest order dispersion (i.e., phase varying quadratically with frequency). Remaining pulse distortions, arising for example due to uncompensated cubic spectral phase (dispersion slope in the terminology of fiber optics), are corrected by using the pulse shaper as a spectral phase equalizer. In the experiments in [108], ~460 fs input pulses at 1542 nm center wavelength are first broadened ten thousand times to ~5 ns in propagating through 50 km of SMF, then recompressed by the DCF to ~14 ps , as shown in Fig. 5.10(a). Although compression by the DCF is roughly 99.7% effective, the residual pulse broadening is still a factor of thirty relative to the bandwidth limit. Most of this broadening is due to a mismatch in fiber lengths, amounting to 120 m of SMF. This can be compensated by programming the pulse shaper for an appropriate quadratic spectral phase, which further compresses the pulse to within a factor of two of the original duration. Compensation of the residual dispersion is achieved by programming the shaper to superimpose an appropriate additional cubic phase variation. An unwrapped view of the total applied phase, comprising almost 100 rad of phase variation, is shown in the inset to Fig. 5.10(a). This leads to a completely recompressed pulse with essentially the original pulse duration (~470 fs) and no observable distortion, Fig. 5.10(b). Thus, in these experiments all-fiber techniques are used for coarse dispersion compensation, while a programmable pulse shaper is used as a spectral phase equalizer to fine tune away any remaining dispersion.

In a completely analogous fashion, programmable pulse shapers are now used extensively in compensation of residual dispersion in femtosecond chirped pulse amplifier systems and in few-cycle pulse generation.

It is worth noting that although the unwrapped spectral phase pictured in Fig. 5.10(a) is quite large, liquid crystal SLMs are in fact limited to relatively small phase shifts, typically a few π. The actual phase function is applied with phase wraps that occur modulo 2π, which fundamentally does not change the pulse shaping operation. However, in the case of SLMs with finite pixel size, a staircase approximation to the desired phase function is obtained. Provided that several SLM pixels are available for each 2π phase variation, the desired phase is well approximated, and high quality pulse shaping (or in this example, dispersion compensation) is possible. Effects related to finite pixel size are discussed, for example, in [1,24].

In addition to experiments with ultrashort pulses, tunable dispersion compensation of conventional laser sources modulated with data in the range 10–40 Gb/s has also been demonstrated via pulse shaping [34,110–112]. In some works, bulk grating spectral dispersers have been replaced with integrated wavelength grating router dispersers for compact implementation, e.g., [111]. Applications of such tunable dispersion compensation include replacing various lengths of conventional dispersion-compensating fibers in 10-Gb/s systems and compensating residual dispersion after the DCF to meet the tight dispersion tolerances required in 40-Gb/s and above based networks. In an example from our lab, programmable compensation of a continuous-wave laser modulated at 10 Gb/s and transmitted through up to 240 km of SMF was achieved [34]. Because the spectral resolution of grating-based pulse shapers is too coarse to conveniently operate within the ~10 GHz optical bandwidth of the modulated data, a hyperfine-resolution pulse shaper was used for this work. The apparatus was constructed using a virtually-imaged phased-array (VIPA) [33] spectral disperser, which enabled programmable pulse shaping over a 50 GHz free spectral range with spectral resolution of approximately 700 MHz. Because the fractional dispersive pulse broadening was much less than

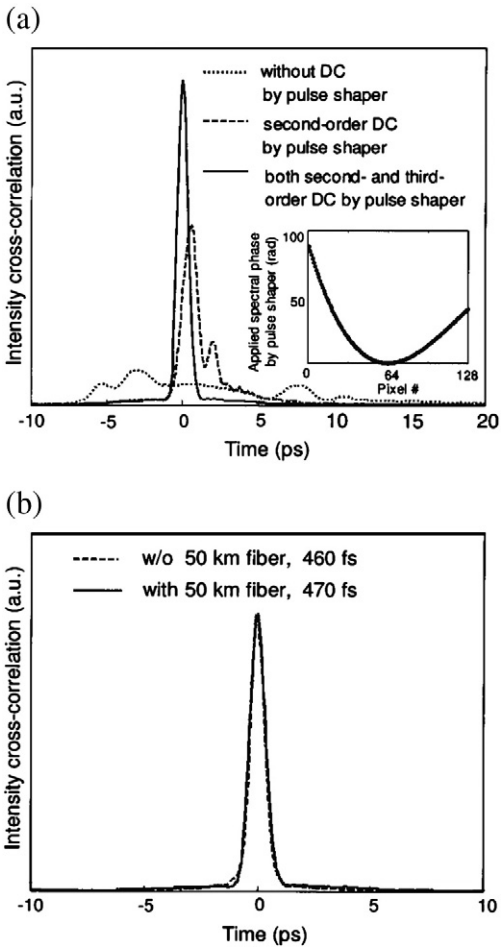

Fig. 5.10. Data from experiments in which <500-fs pulses are transmitted through 50 km of standard single-mode fiber, with subsequent compression using dispersion compensating fiber. (a) Intensity profiles of pulses after various degrees of further compression using the pulse shaper for spectral phase equalization. Inset: applied spectral phase profile for full compression. (b) Comparison of pulses before and after transmission. With spectral phase equalization, the pulse duration is preserved.

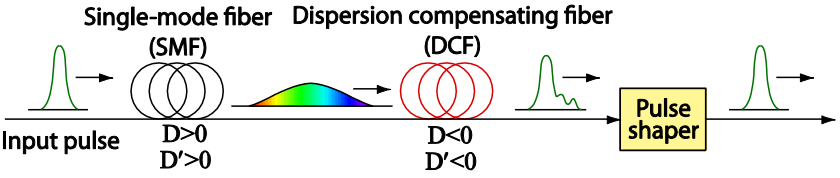

Fig. 5.9. Schematic view of fiber dispersion compensation using a pulse shaper as a programmable spectral phase equalizer. Similar schemes involving pulse shapers are used to compensate residual spectral phase in chirped pulse amplifier systems and few cycle pulse compression experiments.

in the sub-500 fs pulse experiments described earlier, the time-bandwidth product supported by the pulse shaper was sufficient for full compensation of the dispersion, without the need for DCF. An additional attractive feature of many pulse shaper based tunable dispersion compensators is the ability to accomplish dispersion compensation simultaneously (in some cases independently) across multiple wavelength channels.

Pulse shaping has also been explored for compensation of polarization-mode dispersion (PMD), a vector distortion arising from small and essentially random birefringences in single-mode optical fiber [113,114]. Some of the basics of PMD may be understood on the basis of a random wave plate model, illustrated in Fig. 5.11(a). Here each wave plate is assumed to have a differential delay $\Delta\tau$ between its birefringent axes, and different wave plates are assumed to have random rotation angles. The delay experienced by an input signal depends on the input polarization and experiences essentially a random walk process. The mean differential group delay observed at the output scales as $\Delta\tau\sqrt{N}$, where N is the number of wave plates. This corresponds to the finding that in real fibers, the mean differential group delay contributed by PMD scales as the square root of fiber length. PMD-induced impairments of optical fiber transmission systems become especially serious for symbol rates of 40 Gbaud/s and higher.

For small PMD (distortions small compared to the pulse duration), PMD is usually treated in a Taylor series expansion framework in optical frequency. Most work on PMD compensators has adopted this viewpoint. However, when PMD is large (distortions significantly greater than the pulse duration), it produces complex pulse distortions involving a frequency-dependent scrambling of the optical polarization state as well as frequency- and polarization-dependent delays. In this regime the Taylor series expansion breaks down; and an all-order PMD description, in which the signal experiences arbitrary frequency-dependent delay and polarization distortions, is necessary. This view maps nicely onto a pulse shaping approach. Consequently, in work in our laboratory, we have adopted this all-order view and have sought to sense and correct the frequency dependent polarization state and spectral phase, in parallel and on a wavelength by wavelength basis [52,53,115–117].

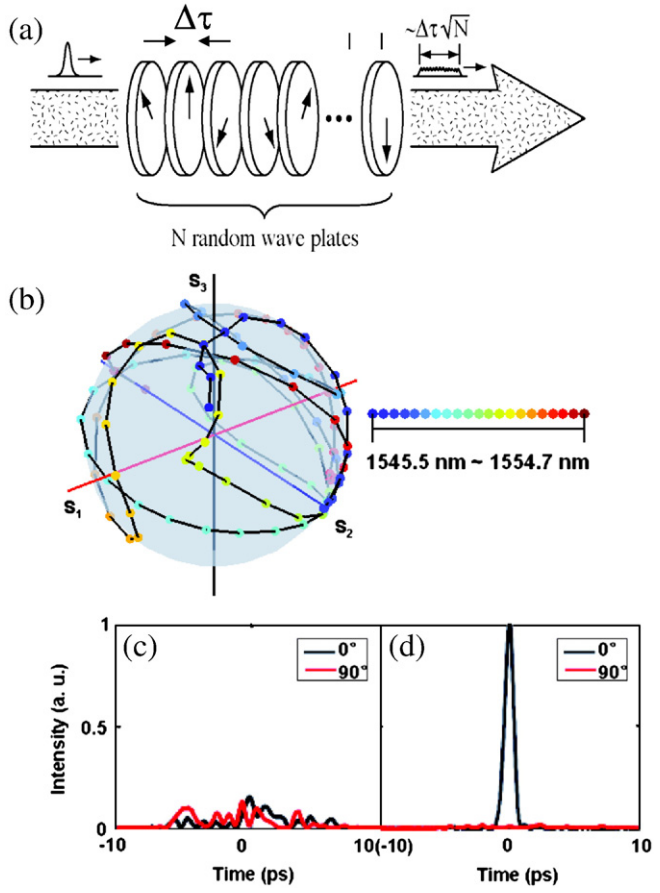

Fig. 5.11. (a) Random wave plate view of polarization mode dispersion (PMD). (b) Poincare sphere plot of frequency-dependent polarization for 800 fs input pulse experiencing strong PMD. The polarization of the input pulse was frequency independent. (c) Intensity profiles of orthogonal polarizations after strong PMD. (d) Restored pulse after pulse shaper based PMD compensator. The output pulse is restored to same duration as the input and has a single, frequency-independent state of polarization.

An example of our experimental results is shown in Fig. 5.11 [52]. Here clean input pulses, with ~800 fs duration and spectral content from 1545 to 1555 nm, are coupled into a home-made PMD emulator with 5.5 ps mean differential group delay. The input pulse prior to the emulator has a frequency-independent polarization, corresponding to a single point on the Poincare sphere (not shown). After the emulator the state of polarization exhibits a complex, frequency dependent trajectory on the Poincare sphere, Fig. 5.11(b), which is characteristic of PMD in the all-order regime. Fig. 5.11(c) shows that approximately equal power is present on orthogonal polarizations; the waveforms for the two polarizations are completely different, although both are spread over a similar (>10 ps) time aperture. Compensation of these effects is accomplished using a pulse shaper provisioned with a custom four layer liquid crystal modulator array, configured such that full correction of frequency-dependent polarization and phase variations can be achieved. Fig. 5.11(d) shows the resulting output pulse. Power is restored to a single polarization state, and the pulse is restored to its original 800 fs duration. In these experiments the pulse shaper is controlled via an open-loop approach based on wavelength-parallel polarimetry [118]. For details, see [52].

The use of pulse shaping for PMD compensation, described above, is closely related to polarization pulse shaping, discussed briefly in Section 4.1. The difference is that in polarization pulse shaping, a bandwidth-limited input pulse in a single polarization state is converted into a user-defined waveform with a time- and frequency-dependent admixture of polarization states. In PMD compensation the opposite is true: one seeks to restore a complicated waveform with time- and frequency-dependent polarization into a bandwidth-limited pulse in a single polarization state.

6. Pulse shaping at high spectral resolution

Unlike conventional modulator technologies, pulse shaping actually gets easier as pulses get shorter — in the sense that with increased optical bandwidth, it becomes easier to separate optical frequency components. Conversely, pulse shaping manipulation of long pulses leads to challenges in spectral resolution. For example, in order to significantly affect a 10 GHz bandwidth lightwave communications signal, a pulse shaper would need a spectral resolution of at most a few GHz. This is near the limit of what is achievable with grating spectral dispersers. In this section we first discuss experiments in which conventional pulse shapers are pushed to very high spectral resolution in order to achieve control of individual spectral lines of a high repetition rate (of order 10 GHz) frequency comb. We then discuss the use of virtually imaged phased array (VIPA) [33] dispersers for even higher resolution shaping, which offers possibilities both for longer time apertures and increased time–bandwidth products.

One motivation for the push toward high resolution pulse shaping is the development of femtosecond frequency combs. Because the output of a mode-locked laser consists of a regular train of pulses, the optical spectrum is actually a comb of sharp spectral lines beneath an envelope that is the spectrum of a single pulse. The spacing between comb lines is equal to the pulse repetition rate, which is easily measurable. However, the absolute frequencies of the comb lines are more

difficult to measure; in the past such absolute frequencies were unknown and left to vary in time. This corresponds to an unknown and varying rigid shift (known as the offset frequency) of the optical comb spectrum. Experimental demonstration of a self-referencing technique that allowed measurement and stabilization of the offset frequency was first reported just over a decade ago [119]. Development of such stabilized frequency combs has led to revolutionary advances in fields such as precision frequency metrology and optical frequency synthesis, e.g., [120–122], an accomplishment for which the Nobel Prize in Physics was awarded in 2005. Key concepts related to the development of mode-locked frequency combs and their applications are discussed, e.g., in [123,124]. In addition, stabilization of the offset frequency means that in the time domain, evolution of the optical phase from pulse to pulse is stable and well defined, offering the new possibility of simultaneous short pulse duration and long term coherence. Bringing pulse shaping and comb technologies together offers prospects for long term coherence with simultaneous control and manipulation of ultrafast time structure, a combination not previously available. This combination, termed either line-by-line pulse shaping or optical arbitrary waveform generation, has potential to enable new applications in areas such as coherent control over quantum mechanical processes, manipulation of high-field laser–matter interactions including attosecond pulse generation, ultra-broadband radio-frequency photonics, telecommunications, and light detection and radar (LIDAR). Recent reviews of optical arbitrary waveform generation may be found in [125,126].

There is a fundamental difference between conventional pulse shaping, in which spectral resolution does not permit addressing of individual lines, and line-by-line shaping. The former case, group-of-lines pulse shaping, is illustrated in Fig. 6.1(a), where f_{rep} is the spacing between comb lines. Assuming that the pulse shaping occurs M lines at a time, the shaped pulses have maximum duration $1/(Mf_{rep})$ and repeat with period $T=1/f_{rep}$. Accordingly, conventional pulse shaping is constrained to produce isolated, low duty factor waveforms. In contrast, for line-by-line pulse shaping ($M=1$), as shown in Fig. 6.1(b), the shaped pulses can overlap, leading to 100% duty factor waveforms in which contributions from different input pulses interfere in the overlapped region [127]. This results in interference effects that depend on the relative phase between pulses, which in turn depends on the comb offset frequency. The sensitivity of the generated waveforms to the offset frequency is fundamentally new in the line-by-line shaping regime and is not observed for group-of-line shaping.

Fig. 6.2 shows a simple demonstration [127]. Line-by-line shaping is achieved by optimizing a grating pulse shaper for a few GHz resolution, which requires beam expansion to several cm, large gratings, and long focal length lens, and by using a comb source with relatively high repetition rate (around 10 GHz). Because self-referenced mode-locked lasers do not easily scale to repetition rates much beyond 1 GHz, these early experiments were performed with a harmonically mode-locked fiber laser (not self-referenced) subject to optical frequency fluctuations. Fig. 6.2 shows data in which the pulse shaper selected a pair of adjacent spectral lines from the spectrum of the laser, operating either at 8.5 GHz or 10.5 GHz. Empirically, the optical frequencies were relatively stable for the lower repetition rate, but showed clear frequency fluctuations for the higher repetition rate. The shaped output exhibits sinusoidal intensity variation in the time domain, with the peak intensity shifted in time according to the relative optical phase shift ($\Phi=0$ or π) applied by the pulse shaper. For 8.5 GHz operation, for which the optical frequencies are relatively stable, overlaid sampling oscilloscope traces show comparable behavior for 0 and π optical phase shifts. In contrast, for 10.5 GHz operation subject to larger optical frequency fluctuations, the shaped waveform is stable for $\Phi=0$ but becomes extremely noisy for $\Phi=\pi$. These effects are direct evidence of interference in the time regions where waveform contributions overlap. For a π phase shift, the original laser pulses (corresponding to $\Phi=0$) are reshaped to form waveforms with intensities in the temporal region where contributions from adjacent input pulses overlap, leading to time-varying interference connected to pulse-to-pulse phase fluctuations. Much weaker fluctuations, if any, are observed at the time locations of the original input pulses, as there is little temporal overlap at those times. Thus, the 100% duty factor property of line-by-line shaping fundamentally gives rise to a new time-dependent noise process that is directly linked to variations in the comb-offset frequency.

Another example of early line-by-line pulse shaping data is shown in Fig. 6.3 [128]. Here pairs of spectral lines with different spacings were selected from the output of a harmonically mode-locked fiber laser spectrally broadened in a nonlinear fiber. With the spectral resolution of the pulse shaper now optimized to ~2.5 GHz, clean suppression of unwanted comb lines with ~30 dB contrast was achieved. As a result waveforms with cosinusoidal intensity variation could be generated in a single apparatus at rates from 10 GHz up to 500 GHz.

Subsequent development has led to demonstrations of complex OAWG with independent control of more than 100 spectral lines. In the experiments of [129], a 5 GHz repetition rate comb was generated by strong electro-optic phase modulation of a continuous-wave laser, which was compressed into a train of 2.4 ps pulses by a first line-by-line shaper, then further compressed and spectrally broadened in a dispersion-decreasing nonlinear fiber. Such electro-optic approaches for generation of high repetition rate combs have become popular for OAWG experiments by a number of groups, as well as for other applications such as optical communications and optical signal processing [30–32,130–138]. The result in [129] was a comb comprising >1000 lines, corresponding in the time domain to a 5 GHz train of pulses only 270 fs in duration, starting from continuous-wave input light! 108 of these lines were selected for subsequent OAWG

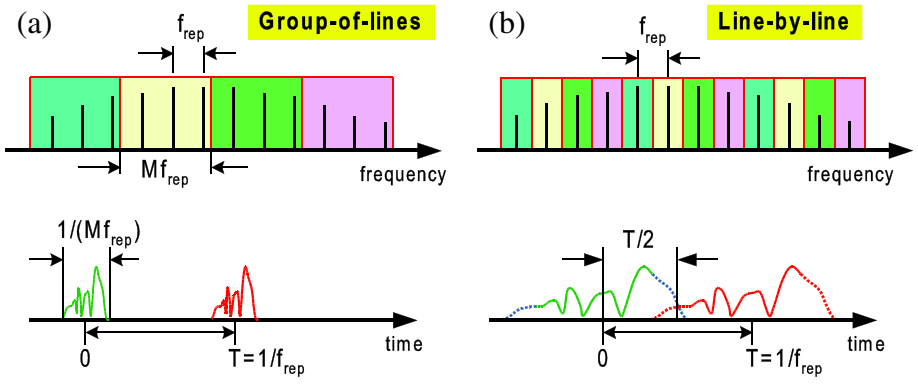

Fig. 6.1. Illustrations of pulse shaping (a) in the group of lines regime, and (b) in the line-by-line regime.

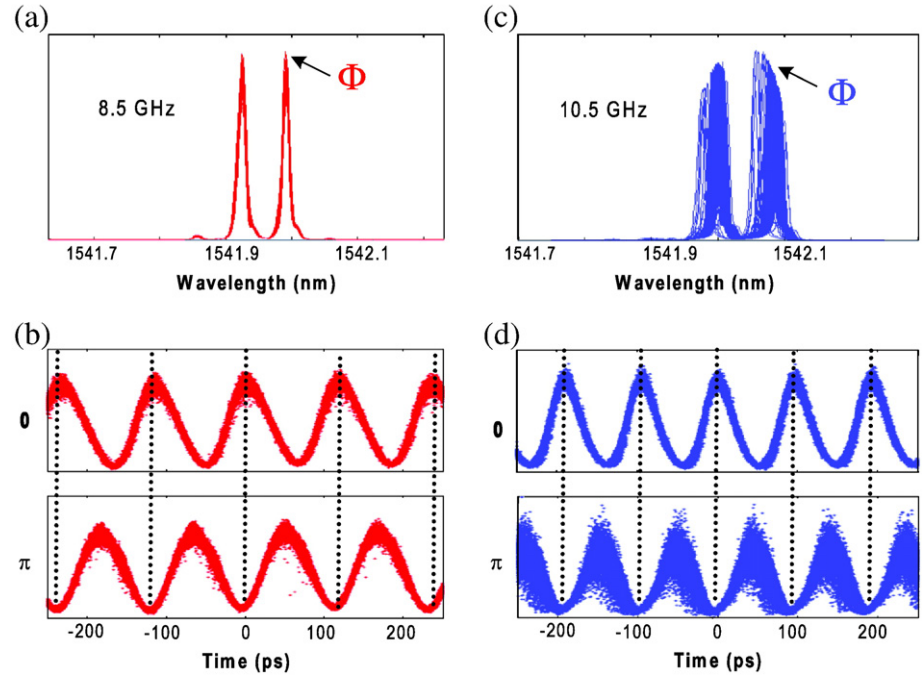

Fig. 6.2. (a) Two relatively stable spectral lines at 8.5 GHz. (b) Overlaid sampling scope traces with phase modulation (0 and π) on one spectral line. (c) Two relatively unstable spectral lines at 10.5 GHz. (d) Overlaid sampling scope traces with phase modulation (0 and π) on one spectral line.

experiments. In an example of OAWG with highly structured temporal features, shown in Fig. 6.4, each pulse is split into two pulses per period, one of which is delayed and the other of which has cubic spectral phase. Fig. 6.4(b,c) show the unwrapped and wrapped discrete spectral phases applied to the 108 comb lines. In this example we chose to program the shaper such that the delayed pulse (linear spectral phase) and the cubic spectral phase pulse correspond to different halves of the spectrum. At some locations the phase change per pixel is π or more — one of the hallmarks of operation in the line-by-line regime. In the time domain trace shown in Fig. 6.4(a), the cubic spectral phase corresponding to quadratic frequency-dependent delay yields a strongly oscillatory tail in the time domain that spans the full waveform period with 100% duty cycle, another hallmark of line-by-line pulse shaping. To confirm OAWG fidelity, the calculated intensity cross-correlations are also shown for comparison. The agreement is excellent everywhere, even in the lowest intensity oscillations.

Recently a grism-based pulse shaper has been used to demonstrate line-by-line shaping of >600 comb lines spaced by 21 GHz over 13 THz of spectrum [139]. The comb source in this work was a mode-locked Ti:sapphire laser, running at a 1 GHz repetition rate compatible with self-referenced operation, that is cavity filtered to increase the line spacing to 21 GHz [140], which is more convenient for line-by-

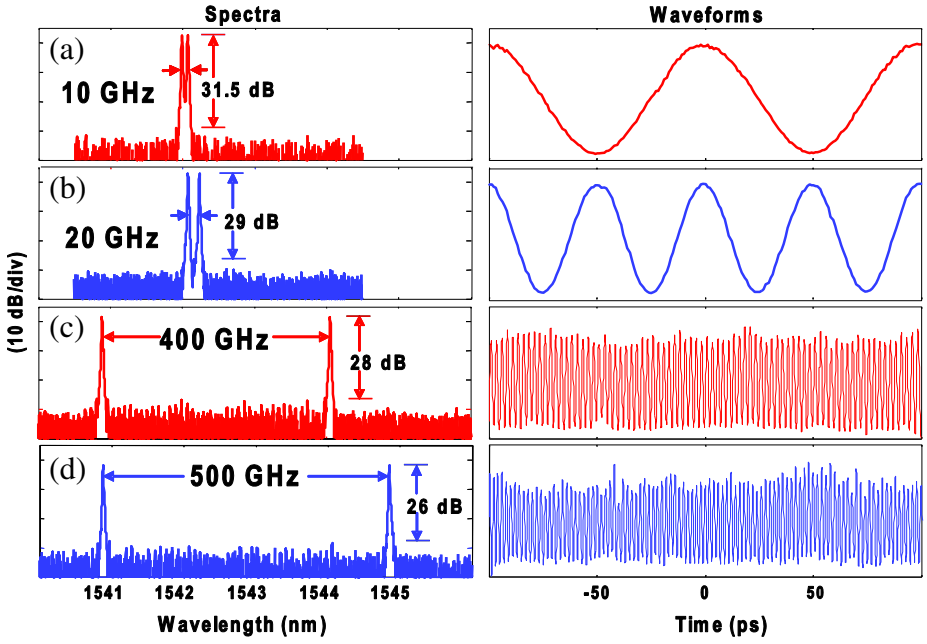

Fig. 6.3. Selecting two spectral lines (separated by a: 10 GHz, b: 20 GHz, c: 400 GHz and d: 500 GHz) and corresponding cosine waveforms (with periods of 100 ps, 50 ps, 2.5 ps and 2 ps). Waveforms for (a,b) are measured using a sampling scope while (c,d) used cross-correlation.

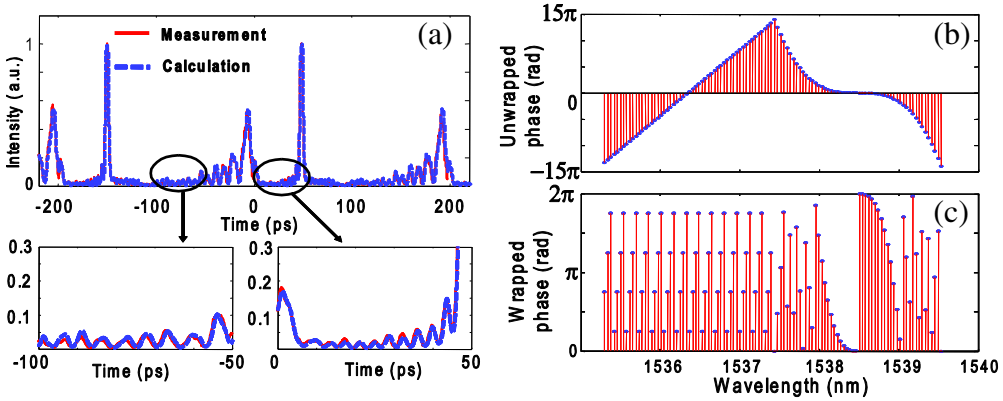

Fig. 6.4. Line-by-line shaping of 108 lines: OAWG with high temporal complexity. (a) The intensity cross-correlation: each pulse is split into two pulses per period, one of which is delayed and the other of which has cubic spectral phase. Each pulse corresponds to one half of the spectrum. Solid line: measured intensity cross-correlation. Dashed line: calculated intensity cross-correlation. (b) The unwrapped spectral phases applied to shaper #2. (c) The wrapped spectral phases applied to shaper #2.

line shaping. A grism is a prism-grating combination that can be optimized to provide near constant angular dispersion over a broad bandwidth [141,142]. This avoids unwanted effects that may arise due to frequency-dependent spectral dispersion in large bandwidth operation [41] and enables precise centering of a large number of individual comb lines on individual pixels of a spatial light modulator.

The high spectral resolution needed for line-by-line shaping has also been achieved using an arrayed waveguide router [30,31,143,144]. Operation in the line-by-line regime is especially suitable for such devices, since the optical comb may be placed at the center of their discrete transmission channels. However, the minimum repetition rate is limited, currently to 10 GHz [144], because increasing the resolution requires increasing the area of the chip, which becomes incompatible with the need for very low phase errors in the waveguide array. This approach also offers potential for integration with other waveguide devices such as modulators. High speed modulation is easier to achieve in a waveguide device than with bulk optical modulators — provided that the waveguides are formed from materials like compound semiconductors, e.g., InP, that support high speed modulation. Recent research includes implementation of an InP tunable integrated pulse shaper with coarse (200 GHz) channel spacing [145] and investigation of fabrication methods suitable for realization of InP-based arrayed waveguide routers with the closer (10–20 GHz) channel spacing appropriate for OAWG [146]. However, to date high fidelity pulse shaping results in the line-by-line regime are limited to silica-based devices that rely on slow thermo-optic modulation.

A continuing research challenge in OAWG is to modulate the individual frequency components at speed sufficiently high that waveforms may be updated on a pulse by pulse basis (otherwise the waveform is limited to repeating every period of the input pulse train). The possibility of operating at a modulation frequency equal exceeding the spectral resolution raises interesting questions about uncertainty in Fourier space, which are addressed theoretically in [147]. An approach to address the competition between resolution and switching speed, in which waveforms are predistorted to account for spectral filtering effects, is suggested in Ref. [148]. To date, however, experimental progress remains limited. A few papers have employed external switching between pairs of shaped waveforms, at speeds comparable to comb repetition rates (~10 GHz), in order to evaluate instrumentation that could be used for single-frame characterization of OAWG waveforms updated on a pulse-by-pulse basis [149–151]. A related switching scheme has been used in conjunction with line-by-line pulse shaping to implement extremely rapid reprogramming of photonically generated RF arbitrary waveforms [152,153].

In addition to the work mentioned above, which specifically involves line-by-line pulse shaping, there are a few reports of waveform switching at rates of tens of MHz to ~1 GHz in group-of-lines pulse shaping experiments. One approach used in these experiments involves pulse shaping masks implemented from arrays of semiconductor-based modulator elements [18,154]. An alternative approach stretches input pulses in a dispersive fiber or chirped Bragg grating, which disperses frequencies in time. Pulse shaping is then accomplished via serial (temporal) modulation of the resulting chirped pulses using a telecommunications modulator, followed by recompression [155].

As mentioned earlier, perhaps the highest spectral resolution in pulse shaping so far has been achieved with a virtually imaged phased array (VIPA) [33]. As shown in Fig. 6.5, the structure of the VIPA is similar to the well known Fabry–Perot etalon, but with some important differences. Instead of symmetric reflectivities, the VIPA typically has a high reflector on the input side ($R \approx 100\%$), with partial reflector (e.g., $r \approx 96\%$) on the output side. Furthermore, light is coupled into the VIPA at a slight angle via cylindrical focusing through an uncoated or anti-reflection coated window. This leads to multiple bounces within the etalon structure, which may be modeled as an array of laterally displaced virtual sources. As a result of the ensuing multiple beam interference, the VIPA acts as a spectral disperser, in the sense that light emerging from the VIPA exhibits a frequency dependent output angle. This may be understood based on the fundamental

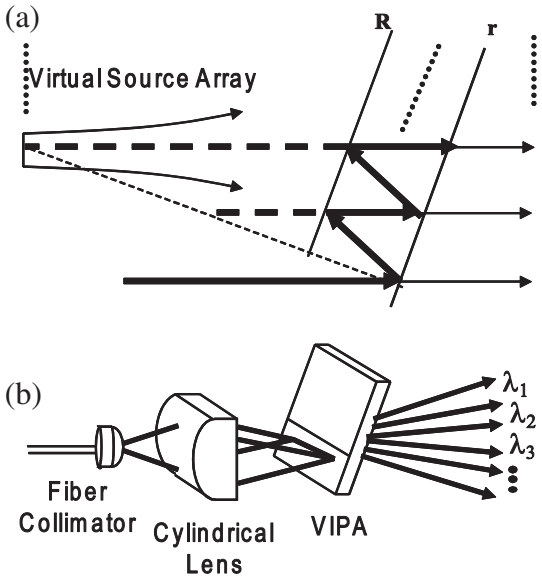

Fig. 6.5. (a) Structure of a virtually imaged phased array (VIPA) device, (b) its use as a spectral disperser.

relationship in ultrafast optics between spectral dispersion and tilted intensity fronts (delay variations across the transverse beam profile) [1,156]. From Fig. 6.5 we immediately observe that the field within the VIPA is delayed by an amount that increases across the transverse beam profile; consequently, the VIPA must function as a spectral disperser. A unique feature of the VIPA as a spectral disperser is its high spectral resolution, similar to that of a Fabry–Perot transmission filter. Detailed analysis of both the spectral dispersion law and spectral resolution of the VIPA may be found in [157,158]. Experimentally, our group has demonstrated 700 MHz spectral resolution both in wavelength demultiplexing experiments and in pulse shaping, using a VIPA with 50 GHz free spectral range [157,158].

Another interesting aspect of the VIPA is that its spectral dispersion function, i.e., the mapping between output angle and frequency, is periodic. The periodicity is known as the free spectral range (FSR) and is determined (as it is for a Fabry–Perot) by the optical delay corresponding to one round trip transit within the device. In a conventional pulse shaping geometry, as in Fig. 2.1, the periodic spectral dispersion means that independent shaping is accomplished only over one FSR of optical bandwidth. In order to retain the high spectral resolution potential of the VIPA while enabling independent shaping over larger bandwidth, it is necessary to separate the different frequency bands corresponding to different FSRs. This has been accomplished with a novel two dimensional (2D) spectral disperser consisting of a diffraction grating and a VIPA arranged to disperse frequencies along orthogonal spatial axes [159]. An attractive feature of this arrangement is that dispersing frequencies into two dimensions allows exploitation of either 2D detector arrays (for spectroscopy) or 2D spatial light modulators (for pulse shaping), such as the LCoS technology discussed in Section 4.1.1. In 2D formats both detector arrays and SLMs offer millions of independent pixels, orders of magnitude higher than in one dimensional formats. The ability to disperse optical frequencies along a 2D grid [159] has already proven useful for monitoring of frequency-dependent polarization effects for fiber communications [160], for massively parallel comb spectroscopy [161], and even for high-speed imaging [162]. A related 2D disperser arrangement consisting of a grating and an arrayed waveguide grating arranged in a cross-dispersion geometry was introduced subsequently and used in research on large channel count optical demultiplexing and wavelength-controlled laser scanning [163,164].

The use of 2D grating-VIPA spectral dispersers for pulse shaping is reported in [64,65]. Fig. 6.6 shows Fourier plane images taken in experiments performed with a 50 MHz repetition rate mode-locked fiber laser source (group-of-lines) pulse shaping, a VIPA with 200 GHz FSR, and a fixed spatial mask [64,65]. Prior to the application of a pulse shaping mask, Fig. 6.6(a), all the frequency components of the input source are present, and the image consists of continuous streaks corresponding to different FSRs of the VIPA spatially separated by the grating. Fig. 6.6(b) shows the Fourier plane image with an amplitude mask designed to introduce both coarse and fine features into the optical spectrum. Alternate 200 GHz FSRs are blocked by the mask and are now missing from the image; within the remaining FSRs alternate 5 GHz pieces of frequency are blocked, leading to the small spots visible within the remaining streaks in the image. Fig. 6.7 shows measurements of the shaped spectrum and intensity profile. The spectrum extends over ~8 THz, with coarse features that repeat every 400 GHz, visible in Fig. 6.7(a), and with fine features of order 5 GHz present within each coarse feature, visible in the expanded view of Fig. 6.7(b). With the 5 GHz minimum feature size, the spectrum contains more than 1600 features, corresponding to substantially higher complexity than previous pulse shaping demonstrations. The combination of broad bandwidth and high spectral resolution corresponds in the time domain to fine temporal features within a broad time aperture. According to the intensity cross-correlation traces, Fig. 6.7(c), the initial 150 fs pulse is now redistributed over a total time aperture of more than 200 ps. The inset in red shows the simulated output which is in excellent agreement with the measurement. The second inset shows the fine temporal features near the main pulse, which arise due to the coarse periodicity in the mask. Even greater pulse shaping complexity is possible using this apparatus, limited in the experiments reported here by the input optical bandwidth. Such 2D pulse shaping arrangements may offer a route toward line-by-line shaping of octave spanning combs, comprising for example 20,000 individual spectral lines for a 10 GHz repetition rate comb centered at 1.5 μm wavelength.

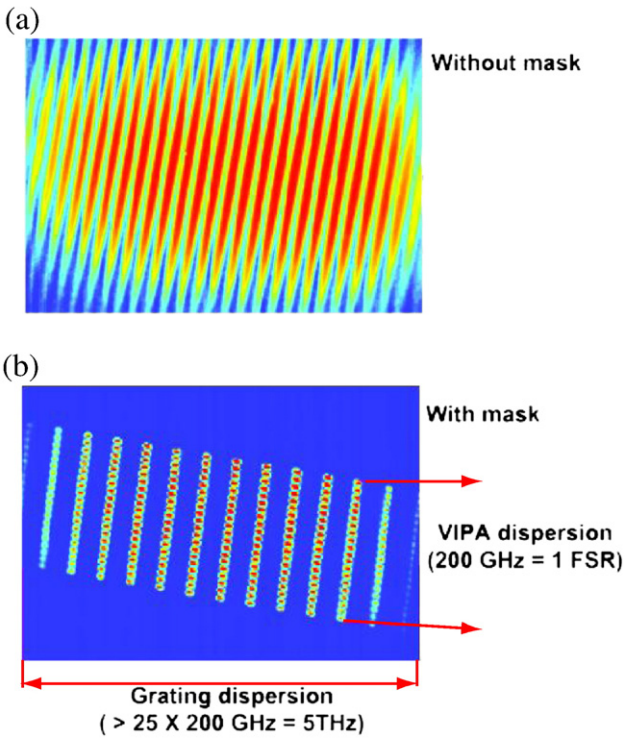

Fig. 6.6. Images of the Fourier plane of a two dimensional VIPA-grating pulse shaper: (a) without a mask, and (b) with a mask.

7. Applications in ultrabroadband radio-frequency photonics

In the area of radio-frequency (RF) photonics, one seeks to use photonics technologies to augment the capabilities of RF electrical or wireless systems [165–167]. Popular applications that have been explored include fiber transmission of high frequency RF signals over distances that would be impossible over electrical cables, optical control of phased-array radars, and photonic implementation of RF filters. In a relatively new subfield of RF photonics, which I refer to as ultrabroadband RF photonics, one seeks to exploit the high speed capabilities of photonic approaches to achieve new functionality for generation and manipulation of ultrawideband (often pulsed) electrical signals, with instantaneous bandwidths beyond those which can be handled by conventional electronic solutions. In this section I describe examples of ultrabroadband RF arbitrary waveform generation as well as ultrabroadband RF phase compensation and pulse compression. Manipulation of broadband RF phase was virtually unexplored in RF photonics until relatively recently.

Optical pulse shaping technology can be directly exploited to realize arbitrary waveform generation capability for ultrawideband radio-frequency (RF) electrical signals. As depicted in Fig. 7.1(a), an ultrashort optical input pulse is first shaped as desired, then directed to a fast optical-to-electrical converter (O/E). By controlling the optical excitation waveform onto the O/E, programmable cycle-by-cycle synthesis of burst RF waveforms can be achieved. In some cases

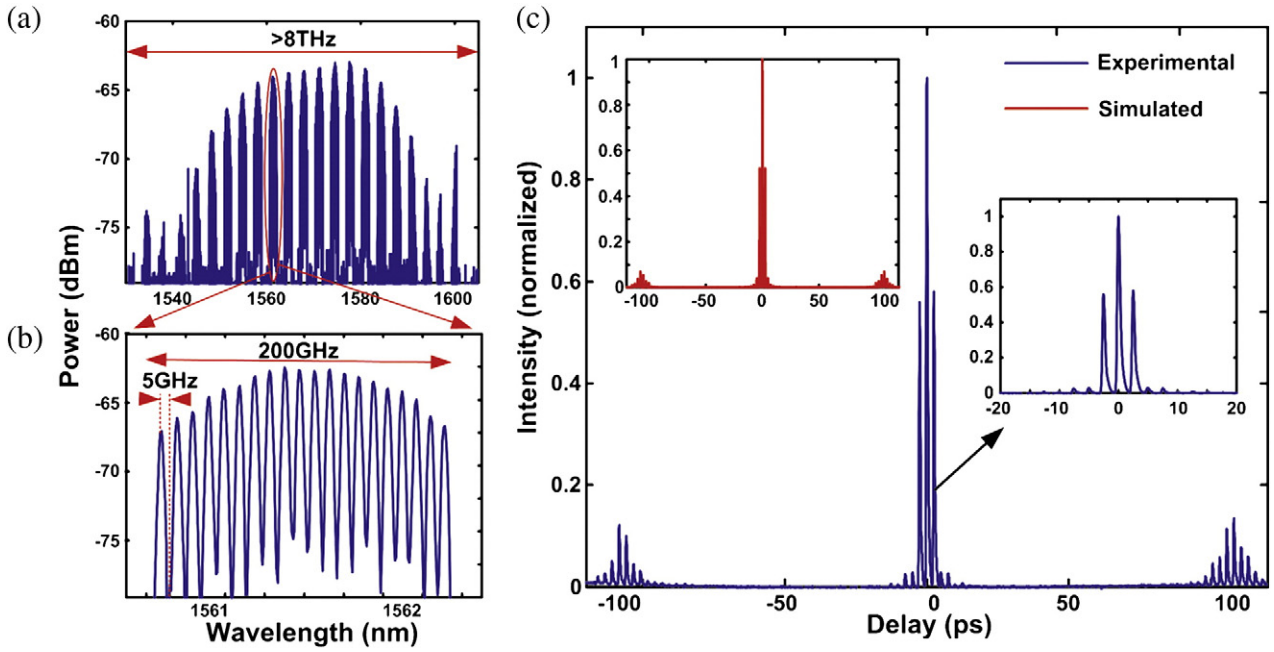

Fig. 6.7. Data obtained using a two dimensional VIPA-grating pulse shaper. (a) Full spectrum and (b) zoomed-in spectrum of a shaped pulse. (c) cross-correlation measurement of shaped intensity profile. An initially bandwidth-limited pulse of 150 fs is shaped over a time aperture exceeding 200 ps.

an optical fiber acts as a dispersive stretcher, or a frequency-to-time converter, in order to match the optical waveform duration to the desired electrical waveform duration [168,169]. This results in a unique technology for generation of waveforms with instantaneous bandwidths far beyond the reach of commercial electronic arbitrary waveform generator solutions, whose bandwidths are limited presently to below 10 GHz. Different choices of pulse shaper configurations, coupled with different choices of O/E converter technologies, has allowed demonstrations of waveform generation from the GHz to the THz. Hence this approach is scalable over several orders of magnitude in RF frequency. An in-depth discussion of some of the earlier work in ultrabroadband RF waveform generation is presented in [170].

Fig. 7.1(b–d) shows examples of subnanosecond RF waveform burst waveforms approximately within the 3.1 to 10.6 GHz band allocated by the FCC for ultrawideband (UWB) wireless communications. These waveforms were generated using the modified generator approach, in which the optical power spectrum of a short optical pulse is tailored using a pulse shaper, followed by optical frequency-to-time conversion in a dispersive medium [168,169]. Fig. 7.1(b) shows a signal with abrupt frequency hops inserted on a cycle-by cycle basis [169], while Fig. 7.1(c,d) show the temporal and spectral profiles of a modulated impulsive signal designed to yield nearly flat RF power spectrum over the full 3.1–10.6 GHz band [171]. The flat power spectrum allows maximized transmitted pulse energy, hence increasing range and signal-to-noise, in a radar or wireless communication system with constrained peak power spectral density. Such waveforms, generated using photonics means over five years ago, substantially exceeded the bandwidth of the electronic waveform generators then available and could only be generated via photonics. Although electronic solutions capable or nearly capable of generating such signals have now become available, photonics scales to much higher frequencies. Examples of waveforms generated using a pulse shaper followed directly by an O/E (no frequency-to-time mapping) are shown in Fig. 7.2. Fig. 7.2(a) shows a burst millimeter-wave signal consisting of 3 cycles at 48 GHz changing abruptly, on a cycle by cycle basis, to 2 cycles at 24 GHz [172]. Also shown is the driving optical waveform; here the 60 GHz bandwidth photodiode acts as a low pass filter, smoothing the optical pulse train into the desired smooth RF electrical waveform. Fig. 7.2(b) shows a periodic millimeter-wave signal with abrupt phase modulations at ~50 GHz [173]. Waveforms such as these are available only via photonic solutions and open up new possibilities for impulsive radar,

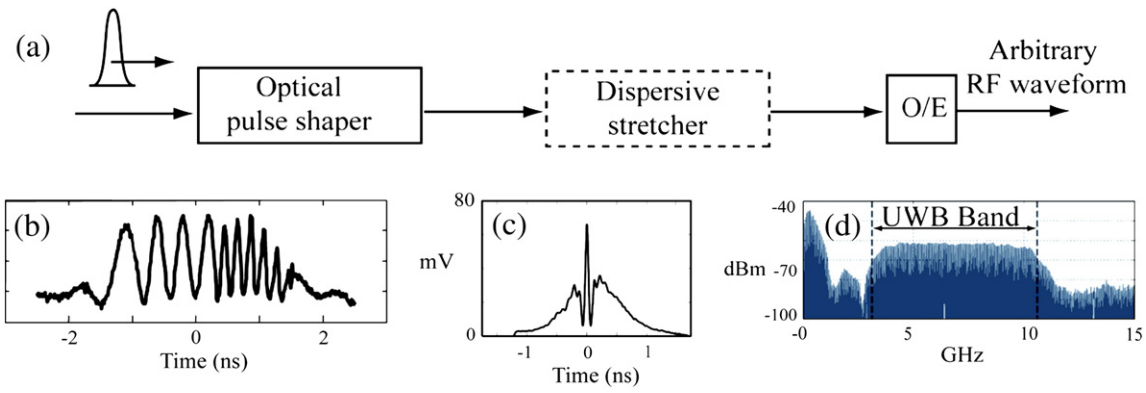

Fig. 7.1. (a) Photonics-enabled RF arbitrary waveform generator, including optional dispersive fiber stretcher. (b) 1.2–2.4–4.9 GHz chirp waveform. (c) Impulsive waveform with fine structure designed to achieve (d) flat RF power spectrum.

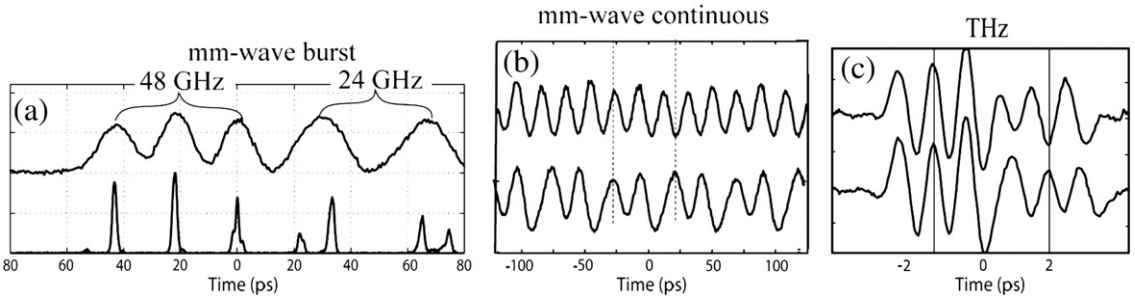

Fig. 7.2. Photonically generated RF waveforms at higher frequencies and bandwidths. (a) 48/24 GHz burst waveform. (b) Periodic and shaped waveforms at 50 GHz: (top) unmodulated sinusoid; (bottom) with abrupt phase modulation. (c) THz waveforms with abrupt phase modulation. In (b) and (c), vertical lines are to visualize the phase modulation.

electronic warfare, RF sensing, and secure wireless communications. Fig. 7.2(c) shows a final example in a still higher frequency (THz) regime [174]. In this case the O/E is a photoconductive antenna. The waveform pair demonstrates the ability to intentionally inject an abrupt phase shift into a THz signal, again something not possible by any other current means.

Although not necessarily clear from the figures, in all of these examples (except for the THz case), the generated RF waveforms are positive definite, since photodetectors respond only to optical intensity. In the THz example, Fig. 7.2(c), the signal is bipolar; the DC component is removed upon radiation by the photoconductive antenna. Radiation and wireless transmission will also remove the DC components in lower frequency bands, since zero frequency signals do not propagate. Alternatively, the DC component may be suppressed by using a setup modified for differential detection, as demonstrated recently in the UWB band [175].

In addition to the use of pulse shapers implemented in bulk optics, as in the work shown above, more compact device alternatives have also been investigated, especially in the RF waveform generation schemes involving shaping in conjunction with frequency-to-time conversion. Fiber Bragg grating technology has been investigated extensively for RF waveform generation [176]. With chirped fiber gratings, the spectral shaping function and the frequency-to-time mapping function are achieved in the same device. Advantages include small form factor and small propagation delay; a limitation is that the pulse shape is determined by the fabricated grating pattern, so programmability is difficult. Recently a programmable spectral shaper chip implemented in silicon photonics has been reported [177]. This device consists of a series of ring resonators independently coupled to through and drop waveguide busses. The resonance frequencies, and the on-resonance transmission amplitudes, may be controlled independently via the thermo-optic effect. This allows for full programmability of the optical spectrum, and hence the generated RF waveform after frequency-to-time mapping and O/E, subject to the number of independent rings (eight in ref. [177]). In the future it may be possible to extend this approach to achieve very fast waveform agility, by incorporating electro-optic (as opposed to thermo-optic) modulators for programming the rings.

RF arbitrary waveform generation enables a number of new experimental possibilities. As one example here we discuss the use of such electrical waveform shaping to allow compensation of dispersive effects due to the antennas used in ultrawideband (UWB) wireless links. This work is closely analogous to the optical dispersion compensation experiments described earlier and constitutes the first hardware implementation of dispersion compensation in the UWB electrical domain. Antenna dispersion, associated with a frequency dependent phase response and hence frequency dependent delay, is an important issue in UWB, as many common antennas that have been optimized for broadband amplitude response do not exhibit linear spectral phase. A related point is that although RF components, including antennas, may be designed for systems that are tunable over a broad frequency range (e.g., 2–18 GHz), they are often not designed for impulsive signals with broad instantaneous bandwidth. The concept of optimizing the antenna feed voltage to obtain desirable temporal properties in the received waveforms, such as peak amplitude or minimal duration, has been explored theoretically [178], but could not previously be tested experimentally due to lack of waveform generation capability. Photonic waveform generator technology has enabled our group to publish the first such experiments [179,180].

An example is shown in Fig. 7.3. First an ~200 ps RF impulse excites a commercial log-periodic antenna for transmission over a short line-of-sight wireless link. The log-periodic antenna, an example of a so-called frequency-independent antenna, exhibits strong dispersion, leading to a ten-fold broadening in the received signal and an obvious frequency sweep. We then generate an intentionally predistorted electrical drive waveform, with frequency dependent delay opposite to that of the dispersive antenna link. The output signal is now recompressed to nearly the original 200 ps duration. Furthermore, the received peak power, normalized to the peak drive

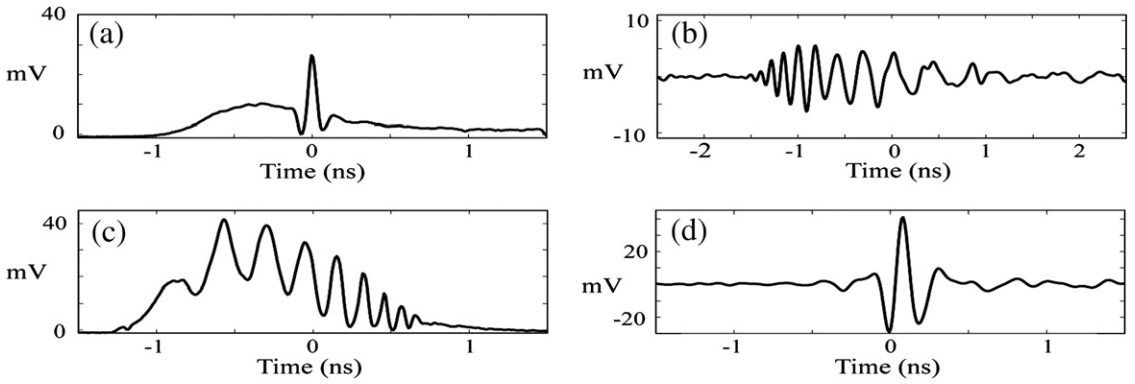

Fig. 7.3. Precompensation of broadband dispersive antenna link. (a) Impulse drive waveform and (b) resulting received signal showing strong pulse distortion. (c) Predistorted drive waveform, resulting in (d) compressed output.

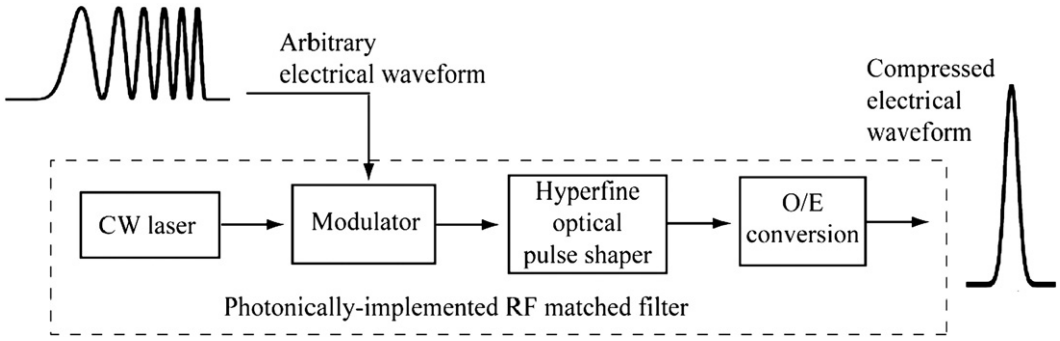

Fig. 7.4. Concept for ultrabroadband RF waveform compression via matched filtering. Here the elements within the box, implemented photonically, together act as a matched filter for an RF electrical signal of interest.

power, is increased nearly 20× (13 dB). Such pulse compression experiments, though common-place in optical systems, are unprecedented in RF systems with the ~10 GHz instantaneous bandwidths considered here. The ability to precompensate antenna distortions should significantly extend the choices of antenna structures that can be applied to UWB wireless.

Ultrabroadband radio-frequency systems will benefit not only from waveform generation technologies but also from new receiver approaches. In particular, analog matched filter receivers capable of compressing frequency swept or other ultrabroadband RF signals to the bandwidth limit are of interest. Compression concentrates energy into a short duration pulse, resulting in an increase in peak power that can aid in signal detection and identification and in interference rejection. Surface acoustic wave (SAW) devices have been used extensively for RF pulse compression. However, such SAW devices are generally not programmable and have been demonstrated only up to 3.63 GHz with 1.1 GHz bandwidth (30% fractional bandwidth), with insertion loss of 23 dB even after accounting for the pulse compression gain [181]. Further progress is difficult due to shrinking dimensions and increased loss associated with higher center frequencies. In modern radar practice, compression is often practiced in the digital domain; however, bandwidth is limited by the ADC technology. In the traditional RF area, the design of arbitrary phase filters remained untouched for many years, especially for ultrabroad bandwidth. Recently microwave chirped delay lines based on chirped Bragg grating structures fabricated onto microwave transmission lines have been reported with bandwidths of several GHz and center frequencies beyond 30 GHz [182–184]. However, the response of such devices is fixed.

A photonics approach based on pulse shaping allows *programmable* phase filtering of RF signals up to ~20 GHz in bandwidth [185]. Fig. 7.4 shows the basic setup for pulse compression operation. A continuous-wave laser is modulated by an arbitrary input RF electrical waveform. This upconverts the RF signal into the optical domain, where in frequency space it represents a broadband sideband adjacent to the original optical carrier. The modulated signal is then passed into a hyperfine-resolution optical pulse shaper for processing. As discussed in a previous section, the pulse shaper employs a VIPA spectral disperser that can separate optical frequencies at much finer resolution (down to ~700 MHz) than conventional pulse shapers (tens of GHz). For the first time this provides sufficient spectral resolution in pulse shaping to address RF filtering applications. The hyperfine pulse shaper is programmed for phase of equal magnitude but opposite sign compared to that of the RF electrical signal of interest. This results in compression of the modulated signal in the optical domain; the overall result after optical-to-electrical conversion is electrical pulse compression. Fig. 7.5 shows an example of photonically implemented, electrical matched filtering data. The uncompressed waveform (Fig. 7.5a) is a 15-bit pseudorandom sequence with 18.7 Gb/s peak modulation rate filling an 800 ps time aperture. The output signal after the photodetector (Fig. 7.5b) is obviously compressed, with duration of only 50 ps (16-fold compression) and 5 times increase in peak voltage (14 dB in power). Exploiting the full programmability of the spectral phase applied by the hyperfine pulse shaper, we have obtained comparable pulse compression results with a range of other waveforms. Experiments in which waveform compression and dispersion compensation are performed simultaneously after transmission over a dispersive antenna link have also been reported [186]. This optical pulse shaping approach constitutes the first technology of any kind capable of generally reconfigurable RF phase filtering over such bandwidths.

8. Conclusion and acknowledgements

In summary, this paper provides a tutorial on the field of femtosecond pulse shaping, with an emphasis on Fourier transform pulse shaping, the most widely applied technique. Pulse shaping permits generation of user defined ultrafast optical waveforms, with control of phase, amplitude, and polarization. This technology has broad applications, with impact both to ultrafast optical science and high-speed photonics. Several examples of applications, selected from the areas of coherent control and lightwave communications, are

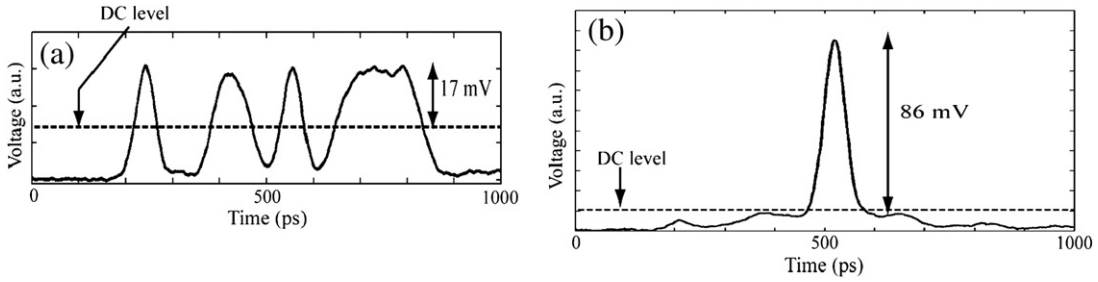

Fig. 7.5. Data demonstrating RF electrical waveform compression. (a) Burst pseudorandom electrical waveform, generated photonically. (b) Output compressed electrical waveform after the matched filter is applied. For display purposes the waveform in (a) is expanded ~1.9× compared to that in (b).

described. Two new research areas in which the author is active, namely, hyperfine spectral resolution pulse shaping and pulse shaping applications in ultrabroadband RF photonics, are discussed and illustrated with examples taken from the author's laboratory.

In the future it is likely that pulse shaping technologies will continue to evolve. New or improved spatial light modulator devices could enable pulse shaping to extend further into the infrared and ultraviolet spectrum, which would facilitate new studies in spectroscopy, while integrated optic pulse shaping implementations and rapidly updatable modulator arrays would enable further applications in lightwave communications. Harnessing the newest SLM technologies with pixel counts beyond one million may contribute to independent shaping of each of the tens of thousands of discrete spectral lines found within octave-spanning frequency comb sources. We may also anticipate that new applications of pulse shaping, that were not previously envisioned, will continue to be introduced.

The author gratefully acknowledges the many students and coworkers over the years with whom he has had the pleasure to collaborate on pulse shaping research. This project was supported in part by the National Science Foundation under grants ECCS-0701448 and ECCS-0925759 and by the Naval Postgraduate School under grant N00244-09-1-0068 under the National Security Science and Engineering Faculty Fellowship program. Any opinion, findings, and conclusions or recommendations expressed in this publication are those of the authors and do not necessarily reflect the views of the sponsors.

References

[1] A.M. Weiner, Ultrafast Optics, Wiley, Hoboken, NJ, 2009.
[2] J.C. Diels, W. Rudolph, Ultrashort Laser Pulse Phenomena, 2nd ed. Academic Press, San Diego, 2006.
[3] C. Froehly, B. Colombeau, M. Vampouille, Shaping and analysis of picosecond light pulses, in: E. Wolf (Ed.), Progress in Optics, North-Holland, Amsterdam, 1983, p. 65.
[4] A.M. Weiner, Rev. Sci. Instr. 71 (2000) 1929.
[5] A. Monmayrant, S. Weber, B. Chatel, J. Physics B Atomic Molecular Optical Physics 43 (2010).
[6] A.M. Weiner, Prog. Quantum Electron. 19 (1995) 161.
[7] A.M. Weiner, J.P. Heritage, Revue Phys. Appl. 22 (1987) 1619.
[8] D. Goswami, Physics Reports 374 (2003) 385.
[9] P. Nuernberger, G. Vogt, T. Brixner, G. Gerber, Phys. Chem. Chem. Phys. 9 (2007) 2470.
[10] Y. Silberberg, Annu. Rev. Phys. Chem. 60 (2009) 277.
[11] A.M. Weiner, A.M. Kan'an, IEEE J. Sel. Top. Quantum Electron. 4 (1998) 317.
[12] A.M. Weiner, Appl. Opt. 47 (2008) A88.
[13] J.P. Heritage, A.M. Weiner, IEEE J. Sel. Top. Quantum Electron. 13 (2007) 1351.
[14] B. Colombeau, M. Vampouille, C. Froehly, Opt. Commun. 19 (1976) 201.
[15] P. Emplit, M. Haelterman, J.-P. Hamaide, Opt. Lett. 18 (1993) 1047.
[16] D.E. Leaird, A.M. Weiner, IEEE J. Quantum Electron. 37 (2001) 494.
[17] D.E. Leaird, A.M. Weiner, Opt. Lett. 29 (2004) 1551.
[18] A. Vega, D.E. Leaird, A.M. Weiner, Opt. Lett. 35 (2010) 1554.
[19] B.H. Kolner, IEEE J. Quantum Electron. 30 (1994) 1951.
[20] C.V. Bennett, B.H. Kolner, Opt. Lett. 24 (1999) 783.
[21] A.M. Weiner, J.P. Heritage, E.M. Kirschner, J. Opt. Soc. Am. B 5 (1988) 1563.
[22] O.E. Martinez, J.P. Gordon, R.L. Fork, J. Opt. Soc. Am. A 1 (1984) 1003.
[23] A.M. Weiner, D.E. Leaird, J.S. Patel, J.R. Wullert, Opt. Lett. 15 (1990) 326.
[24] A.M. Weiner, D.E. Leaird, J.S. Patel, J.R. Wullert, IEEE J. Quantum Electron. 28 (1992) 908.
[25] M.M. Wefers, K.A. Nelson, Opt. Lett. 20 (1995) 1047.
[26] M.A. Dugan, J.X. Tull, W.S. Warren, J. Opt. Soc. Am. B 14 (1997) 2348.
[27] E. Zeek, K. Maginnis, S. Backus, U. Russek, M. Murnane, G. Mourou, H. Kapteyn, G. Vdovin, Opt. Lett. 24 (1999) 493.
[28] A.M. Weiner, D.E. Leaird, Opt. Lett. 15 (1990) 51.
[29] R.D. Nelson, D.E. Leaird, A.M. Weiner, Opt. Express 11 (2003) 1763.
[30] D. Miyamoto, K. Mandai, T. Kurokawa, S. Takeda, T. Shioda, H. Tsuda, IEEE Photonics Technol. Lett. 18 (2006) 721.
[31] N.K. Fontaine, R.P. Scott, J. Cao, A. Karalar, W. Jiang, K. Okamoto, J.P. Heritage, B.H. Kolner, S.J.B. Yoo, Opt. Lett. 32 (2007) 865.
[32] R.P. Scott, N.K. Fontaine, J. Cao, K. Okamoto, B.H. Kolner, J.P. Heritage, S.J.B. Yoo, Opt. Express 15 (2007) 9977.
[33] M. Shirasaki, Opt. Lett. 21 (1996) 366.
[34] G.H. Lee, S.J. Xiao, A.M. Weiner, IEEE Photonics Technol. Lett. 18 (2006) 1819.
[35] S. Xiao, A.M. Weiner, IEEE Photonics Technol. Lett. 17 (2005) 372.
[36] M.Y. Shverdin, D.R. Walker, D.D. Yavuz, G.Y. Yin, S.E. Harris, Phys. Rev. Lett. 94 (2005).
[37] T. Binhammer, E. Rittweger, R. Ell, F.X. Kartner, U. Morgner, IEEE J. Quantum Electron. 41 (2005) 1552.
[38] D.H. Reitze, A.M. Weiner, D.E. Leaird, Appl. Phys. Lett. 61 (1992) 1260.
[39] L. Wang, A.M. Weiner, Opt. Commun. 167 (1999) 211.
[40] A. Pe'er, B. Dayan, A.A. Friesem, Y. Silberberg, Phys. Rev. Lett. 94 (2005).
[41] H. Wang, Z. Zheng, D.E. Leaird, A.M. Weiner, T.A. Dorschner, J.J. Fijol, L.J. Friedman, H.Q. Nguyen, L.A. Palmaccio, IEEE J. Sel. Top. Quantum Electron. 7 (2001) 718.
[42] M.M. Wefers, K.A. Nelson, IEEE J. Quantum Electron. 32 (1996) 161.
[43] R.N. Thurston, J.P. Heritage, A.M. Weiner, W.J. Tomlinson, IEEE J. Quantum Electron. 22 (1986) 682.
[44] H.P. Sardesai, C.-C. Chang, A.M. Weiner, J. Lightwave Technol. 16 (1998) 1953.
[45] J.A. Salehi, A.M. Weiner, J.P. Heritage, J. Lightwave Technol. 8 (1990) 478.
[46] A.M. Weiner, Z. Jiang, D.E. Leaird, J. Optical Networking 6 (2007) 728.
[47] P.G. deGennes, The Physics of Liquid Crystals, Clarendon, Oxford, 1974.
[48] T. Brixner, G. Gerber, Opt. Lett. 26 (2001) 557.
[49] O. Masihzadeh, P. Schlup, R.A. Bartels, Opt. Express 15 (2007) 18025.
[50] M. Ninck, A. Galler, T. Feurer, T. Brixner, Opt. Lett. 32 (2007) 3379.
[51] F. Weise, A. Lindinger, Opt. Lett. 34 (2009) 1258.
[52] H.X. Miao, A.M. Weiner, L. Mirkin, P.J. Miller, Opt. Lett. 32 (2007) 2360.
[53] H. Miao, A.M. Weiner, L. Mirkin, P.J. Miller, IEEE Photonics Technol. Lett. 20 (2008) 545.
[54] Q.Q. Mu, Z.L. Cao, L.F. Hu, D.Y. Li, L. Xuan, Opt. Express 14 (2006) 8013.
[55] J.E. Wolfe, R.A. Chipman, Appl. Opt. 45 (2006) 1688.
[56] X.H. Wang, B. Wang, J. Pouch, F. Miranda, J.E. Anderson, P.J. Bos, Opt. Eng. 43 (2004) 2769.
[57] J.W. Wilson, P. Schlup, R.A. Bartels, Opt. Express 15 (2007) 8979.
[58] E. Frumker, Y. Silberberg, Opt. Lett. 32 (2007) 1384.
[59] J.C. Vaughan, T. Hornung, T. Feurer, K.A. Nelson, Opt. Lett. 30 (2005) 323.
[60] T. Feurer, J.C. Vaughan, R.M. Koehl, K.A. Nelson, Opt. Lett. 27 (2002) 652.
[61] R.P. Scott, W. Cong, V.J. Hernandez, K.B. Li, B.H. Kolner, J.P. Heritage, S.J. Ben Yoo, J. Lightwave Technol. 23 (2005) 3232.
[62] T. Hornung, J.C. Vaughan, T. Feurer, K.A. Nelson, Opt. Lett. 29 (2004) 2052.
[63] E. Frumker, D. Oron, D. Mandelik, Y. Silberberg, Opt. Lett. 29 (2004) 890.
[64] V.R. Supradeepa, C.B. Huang, D.E. Leaird, A.M. Weiner, Opt. Express 16 (2008) 11878.
[65] V.R. Supradeepa, D.E. Leaird, A.M. Weiner, in: M. Chergui, D.M. Jonas, E. Riedle, R.W. Schoenlein, A.J. Taylor (Eds.), Ultrafast Phenomena XVII, Oxford University Press, Snowmass, CO, 2010, p. 811.
[66] G. Baxter, S. Frisken, D. Abakoumov, H. Zhou, I. Clarke, A. Bartos, S. Poole, 2006 Optical Fiber Communication Conference/National Fiber Optic Engineers Conference, vols. 1–6, 2006, p. 94.
[67] N.A.F. Roelens, S. Frisken, J.A. Bolger, D. Abakoumov, G. Baxter, S. Poole, B.J. Eggleton, J. Lightwave Technol. 26 (2008) 73.
[68] P.F. Tian, D. Keusters, Y. Suzaki, W.S. Warren, Science 300 (2003) 1553.
[69] B.J. Pearson, T.C. Weinacht, Opt. Express 15 (2007) 4385.
[70] S.H. Shim, D.B. Strasfeld, E.C. Fulmer, M.T. Zanni, Opt. Lett. 31 (2006) 838.
[71] P. Tournois, Opt. Commun. 140 (1997) 245.
[72] F. Verluise, V. Laude, Z. Cheng, C. Spielmann, P. Tournois, Opt. Lett. 25 (2000) 575.
[73] S.E. Harris, R.W. Wallace, J. Opt. Soc. Am. 59 (1969) 744.
[74] D.A. Smith, J.E. Baran, J.J. Johnson, K.-W. Cheung, IEEE J. Sel. Areas Commun. 8 (1990) 1151.
[75] M.E. Fermann, V.D. Silva, D.A. Smith, Y. Silberberg, A.M. Weiner, Opt. Lett. 18 (1993) 1505.
[76] N. Krebs, R.A. Probst, E. Riedle, Opt. Express 18 (2010) 6164.
[77] D. Yelin, D. Meshulach, Y. Silberberg, Opt. Lett. 22 (1997) 1793.
[78] D. Meshulach, D. Yelin, Y. Silberberg, J. Opt. Soc. Am. B 15 (1998) 1615.
[79] T. Baumert, T. Brixner, V. Seyfried, M. Strehle, G. Gerber, Appl. Phys. B 65 (1997) 779.
[80] R.S. Judson, H. Rabitz, Phys. Rev. Lett. 68 (1992) 1500.
[81] A. Assion, T. Baumert, M. Bergt, T. Brixner, B. Kiefer, V. Seyfried, M. Strehle, G. Gerber, Science 282 (1998) 919.
[82] C.J. Bardeen, V.V. Yakovlev, K.R. Wilson, S.D. Carpenter, P.M. Weber, W.S. Warren, Chem. Phys. Lett. 280 (1997) 151.
[83] T. Brixner, N.H. Damrauer, P. Niklaus, G. Gerber, Nature 414 (2001) 57.
[84] R.J. Levis, G.M. Menkir, H. Rabitz, Science 292 (2001) 709.
[85] R. Bartels, S. Backus, E. Zeek, L. Misoguti, G. Vdovin, I.P. Christov, M.M. Murnane, H.C. Kapteyn, Nature 406 (2000) 164.
[86] F.G. Omenetto, A.J. Taylor, M.D. Moores, D.H. Reitze, Opt. Lett. 26 (2001) 938.
[87] J.L. Herek, W. Wohlleben, R.J. Cogdell, D. Zeidler, M. Motzkus, Nature 417 (2002) 533.
[88] M. Aeschlimann, M. Bauer, D. Bayer, T. Brixner, F.J. de Abajo, W. Pfeiffer, M. Rohmer, C. Spindler, F. Steeb, Nature 446 (2007) 301.
[89] M. Aeschlimann, M. Bauer, D. Bayer, T. Brixner, S. Cunovic, F. Dimler, A. Fischer, W. Pfeiffer, M. Rohmer, C. Schneider, F. Steeb, C. Struber, D.V. Voronine, Proc. Natl. Acad. Sci. U.S.A. 107 (2010) 5329.
[90] Y.-X. Yan, E.B. Gamble, K.A. Nelson, J. Chem. Phys. 83 (1985) 5391.
[91] S. Desilvestri, J.G. Fujimoto, E.P. Ippen, E.B. Gamble, L.R. Williams, K.A. Nelson, Chem. Phys. Lett. 116 (1985) 146.
[92] A.M. Weiner, D.E. Leaird, G.P. Wiederrecht, K.A. Nelson, Science 247 (1990) 1317.
[93] A.M. Weiner, D.E. Leaird, G.P. Wiederrecht, K.A. Nelson, J. Opt. Soc. Am. B 8 (1991) 1264.
[94] N. Dudovich, D. Oron, Y. Silberberg, Nature 418 (2002) 512.
[95] D. Meshulach, Y. Silberberg, Nature 396 (1998) 239.
[96] Z. Zheng, A.M. Weiner, Opt. Lett. 25 (2000) 984.
[97] Z. Zheng, A.M. Weiner, Chem. Phys. 267 (2001) 161.
[98] K.R. Parameswaran, R.K. Route, J.R. Kurz, R.V. Roussev, M.M. Fejer, M. Fujimura, Opt. Lett. 27 (2002) 179.
[99] Z. Jiang, D.S. Seo, S.D. Yang, D.E. Leaird, R.V. Roussev, C. Langrock, M.M. Fejer, A.M. Weiner, IEEE Photonics Technol. Lett. 16 (2004) 1778.

[100] V.V. Lozovoy, I. Pastirk, M. Dantus, Opt. Lett. 29 (2004) 775.
[101] B.W. Xu, J.M. Gunn, J.M. Dela Cruz, V.V. Lozovoy, M. Dantus, J. Opt. Soc. Am. B 23 (2006) 750.
[102] H. Wang, Y. Wu, C.Q. Li, H. Mashiko, S. Gilbertson, Z.H. Chang, Opt. Express 16 (2008) 14448.
[103] B.W. Xu, Y. Coello, V.V. Lozovoy, D.A. Harris, M. Dantus, Opt. Express 14 (2006) 10939.
[104] J.E. Ford, K.W. Goossen, J.A. Walker, D.T. Neilson, D.M. Tennant, S.Y. Park, J.W. Sulhoff, IEEE J. Sel. Top. Quantum Electron. 10 (2004) 579.
[105] J.E. Ford, V.A. Aksyuk, D.J. Bishop, J.A. Walker, J. Lightwave Technol. 17 (1999) 904.
[106] J.S. Patel, Y. Silberberg, IEEE Photonics Technol. Lett. 7 (1995) 514.
[107] C.-C. Chang, H.P. Sardesai, A.M. Weiner, Opt. Lett. 23 (1998) 283.
[108] Z. Jiang, S.D. Yang, D.E. Leaird, A.M. Weiner, Opt. Lett. 30 (2005) 1449.
[109] S. Shen, A.M. Weiner, IEEE Photonics Technol. Lett. 11 (1999) 827.
[110] T. Sano, T. Iwashima, M. Katayama, T. Kanie, M. Harumoto, M. Shigehara, H. Suganuma, M. Nishimura, IEEE Photonics Technol. Lett. 15 (2003) 1109.
[111] D.M. Marom, C.R. Doerr, M.A. Cappuzzo, E.Y. Chen, A. Wong-Foy, L.T. Gomez, S. Chandrasekhar, J. Lightwave Technol. 24 (2006) 237.
[112] H. Ooi, K. Nakamura, Y. Akiyama, T. Takahara, T. Terahara, Y. Kawahata, H. Isono, G. Ishikawa, J. Lightwave Technol. 20 (2002) 2196.
[113] C.D. Poole, J. Nagel, in: I.P. Kaminow, T.L. Koch (Eds.), Optical Fiber Telecommunications, Academic Press, San Diego, 1997.
[114] H. Kogelnik, R.M. Jopson, L.E. Nelson, in: I. Kaminow, T. Li (Eds.), Optical Fiber Telecommunications IVB, Academic Press, San Diego, 2002.
[115] M. Akbulut, A.M. Weiner, P.J. Miller, Opt. Lett. 30 (2005) 2691.
[116] M. Akbulut, A.M. Weiner, P.J. Miller, J. Lightwave Technol. 24 (2006) 251.
[117] L. Xu, H.X. Miao, A.M. Weiner, IEEE Photonics Technol. Lett. 22 (2010) 1078.
[118] S.X. Wang, A.M. Weiner, Opt. Lett. 29 (2004) 923.
[119] D.J. Jones, S.A. Diddams, J.K. Ranka, A. Stentz, R.S. Windeler, J.L. Hall, S.T. Cundiff, Science 288 (2000) 635.
[120] R. Holzwarth, T. Udem, T.W. Hansch, J.C. Knight, W.J. Wadsworth, P.S.J. Russell, Phys. Rev. Lett. 85 (2000) 2264.
[121] T. Udem, R. Holzwarth, T.W. Hansch, Nature 416 (2002) 233.
[122] L.S. Ma, Z.Y. Bi, A. Bartels, L. Robertsson, M. Zucco, R.S. Windeler, G. Wilpers, C. Oates, L. Hollberg, S.A. Diddams, Science 303 (2004) 1843.
[123] S.T. Cundiff, J. Phys. D Appl. Phys. 35 (2002) R43.
[124] J. Ye, S.T. Cundiff, Femtosecond Optical Frequency Comb Technology, Springer, 2005.
[125] S.T. Cundiff, A.M. Weiner, Nat. Photonics 4 (2010) 760.
[126] C.B. Huang, Z. Jiang, D.E. Leaird, J. Caraquitena, A.M. Weiner, Laser Photonics Rev. 2 (2008) 227.
[127] Z. Jiang, D.S. Seo, D.E. Leaird, A.M. Weiner, Opt. Lett. 30 (2005) 1557.
[128] Z. Jiang, D.E. Leaird, A.M. Weiner, Opt. Express 13 (2005) 10431.
[129] Z. Jiang, C.B. Huang, D.E. Leaird, A.M. Weiner, Nat. Photonics 1 (2007) 463.
[130] H. Murata, A. Morimoto, T. Kobayashi, S. Yamamoto, IEEE J. Sel. Top. Quantum Electron. 6 (2000) 1325.
[131] M. Fujiwara, M. Teshima, J. Kani, H. Suzuki, N. Takachio, K. Iwatsuki, J. Lightwave Technol. 21 (2003) 2705.
[132] T. Ohara, H. Takara, T. Yamamoto, H. Masuda, T. Morioka, M. Abe, H. Takahashi, J. Lightwave Technol. 24 (2006) 2311.
[133] Z. Jiang, D.E. Leaird, C.B. Huang, H.X. Miao, M. Kourogi, K. Imai, A.M. Weiner, IEEE J. Quantum Electron. 43 (2007) 1163.
[134] R.P. Scott, N.K. Fontaine, J.P. Heritage, B.H. Kolner, S.J.B. Yoo, Optical Fiber Communication and the National Fiber Optic Engineers Conference, 2007.
[135] I. Morohashi, T. Sakamoto, H. Sotobayashi, T. Kawanishi, L. Hosako, M. Tsuchiya, Opt. Lett. 33 (2008) 1192.
[136] S. Ozharar, F. Quinlan, I. Ozdur, S. Gee, P.J. Delfyett, IEEE Photonics Technol. Lett. 20 (2008) 36.
[137] T. Yamamoto, T. Komukai, K. Suzuki, A. Takada, J. Lightwave Technol. 27 (2009) 4297.
[138] R. Wu, V.R. Supradeepa, C.M. Long, D.E. Leaird, A.M. Weiner, Opt. Lett. 35 (2010) 3234.
[139] M.S. Kirchner, S.A. Diddams, Opt. Lett. 35 (2010) 3264.
[140] M.S. Kirchner, D.A. Braje, T.M. Fortier, A.M. Weiner, L. Hollberg, S.A. Diddams, Opt. Lett. 34 (2009) 872.
[141] S. Kane, J. Squier, J. Opt. Soc. Am. B 14 (1997) 661.
[142] W.A. Traub, J. Opt. Soc. Am. A 7 (1990) 1779.
[143] K. Takiguchi, K. Okamoto, I. Kominato, H. Takahashi, T. Shibata, Electron. Lett. 40 (2004) 537.
[144] N.K. Fontaine, R.P. Scott, C.X. Yang, D.J. Geisler, J.P. Heritage, K. Okamoto, S.J.B. Yoo, Opt. Lett. 33 (2008) 1714.
[145] M.J.R. Heck, P. Munoz, B.W. Tilma, E. Bente, Y. Barbarin, Y.S. Oei, R. Notzel, M.K. Smit, IEEE J. Quantum Electron. 44 (2008) 370.
[146] J.H. Baek, F.M. Soares, S.W. Seo, W. Jiang, N.K. Fontaine, R.G. Broeke, J. Cao, F. Olsson, S. Lourdudoss, S.J.B. Yoo, IEEE Photonics Technol. Lett. 21 (2009) 298.
[147] J.T. Willits, A.M. Weiner, S.T. Cundiff, Opt. Express 16 (2008) 315.
[148] D.J. Geisler, N.K. Fontaine, T.T. He, R.P. Scott, L. Paraschis, J.P. Heritage, S.J.B. Yoo, Opt. Express 17 (2009) 15911.
[149] V.R. Supradeepa, D.E. Leaird, A.M. Weiner, Opt. Express 17 (2009) 14434.
[150] N.K. Fontaine, R.P. Scott, J.P. Heritage, S.J.B. Yoo, Opt. Express 17 (2009) 12332.
[151] N.K. Fontaine, R.P. Scott, L.J. Zhou, F.M. Soares, J.P. Heritage, S.J.B. Yoo, Nat. Photonics 4 (2010) 248.
[152] C.-B. Huang, D.E. Leaird, A.M. Weiner, Opt. Lett. 32 (2007) 3242.
[153] C.B. Huang, D.E. Leaird, A.M. Weiner, IEEE Photonics Technol. Lett. 21 (2009) 1287.
[154] E. Frumker, E. Tal, Y. Silberberg, D. Majer, Opt. Lett. 30 (2005) 2796.
[155] S. Thomas, A. Malacarne, F. Fresi, L. Poti, J. Azana, J. Lightwave Technol. 28 (2010) 1832.
[156] Z. Bor, B. Racz, Opt. Commun. 54 (1985) 165.
[157] S. Xiao, A.M. Weiner, C. Lin, J. Lightwave Technol. 23 (2005) 1456.
[158] S.J. Xiao, A.M. Weiner, C. Lin, IEEE J. Quantum Electron. 40 (2004) 420.
[159] S.J. Xiao, A.M. Weiner, Opt. Express 12 (2004) 2895.
[160] S.X. Wang, S.J. Xiao, A.M. Weiner, Opt. Express 13 (2005) 9374.
[161] S.A. Diddams, L. Hollberg, V. Mbele, Nature 445 (2007) 627.
[162] K. Goda, K.K. Tsia, B. Jalali, Nature 458 (2009) 1145.
[163] T. Chan, E. Myslivets, J.E. Ford, Opt. Express 16 (2008) 14617.
[164] T.K. Chan, J. Karp, R. Jiang, N. Alic, S. Radic, C.F. Marki, J.E. Ford, J. Lightwave Technol. 25 (2007) 719.
[165] J. Capmany, D. Novak, Nat. Photonics 1 (2007) 319.
[166] R.A. Minasian, IEEE Trans. Microwave Theory Tech. 54 (2006) 832.
[167] J.P. Yao, J. Lightwave Technol. 27 (2009) 314.
[168] J. Chou, Y. Han, B. Jalali, IEEE Photonics Technol. Lett. 15 (2003) 581.
[169] I.S. Lin, J.D. McKinney, A.M. Weiner, IEEE Microwave Wireless Compon. Lett. 15 (2005) 226.
[170] J.D. McKinney, A.M. Weiner, Photonic Synthesis of Ultrabroadband Arbitrary Electromagnetic Waveforms, in: C.H. Lee (Ed.), Advances in Microwave Photonics, CRC Press, Boca Raton, 2006.
[171] J.D. McKinney, I.S. Lin, A.M. Weiner, IEEE Trans. Microwave Theory Tech. 54 (2006) 4247.
[172] J.D. McKinney, D.E. Leaird, A.M. Weiner, Opt. Lett. 27 (2002) 1345.
[173] J.D. McKinney, D.S. Seo, D.E. Leaird, A.M. Weiner, J. Lightwave Technol. 21 (2003) 3020.
[174] Y. Liu, S.-G. Park, A.M. Weiner, IEEE J. Sel. Top. Quantum Electron. 2 (1996) 709.
[175] J.D. McKinney, IEEE Photonics Technol. Lett. 22 (2010) 1193.
[176] J.P. Yao, F. Zeng, Q. Wang, J. Lightwave Technol. 25 (2007) 3219.
[177] M.H. Khan, H. Shen, Y. Xuan, L. Zhao, S.J. Xiao, D.E. Leaird, A.M. Weiner, M.H. Qi, Nat. Photonics 4 (2010) 117.
[178] D.M. Pozar, IEEE Trans. Antennas Propag. 51 (2003) 2335.
[179] J.D. McKinney, D. Peroulis, A.M. Weiner, IEEE Trans. Microwave Theory Tech. 56 (2008) 710.
[180] J.D. McKinney, A.M. Weiner, IEEE Trans. Microwave Theory Tech. 54 (2006) 1681.
[181] R. Brocato, J. Skinner, G. Wouters, J. Wendt, E. Heller, J. Blaich, IEEE Trans. Ultrason., Ferroelectr., Freq. Control 53 (2006) 1554.
[182] M.A.G. Laso, T. Lopetegi, M.J. Erro, D. Benito, M.J. Garde, M.A. Muriel, M. Sorolla, M. Guglielmi, IEEE Microwave Wireless Compon. Lett. 11 (2001) 486.
[183] J.D. Schwartz, J. Azana, D.V. Plant, IEEE Microwave Wireless Compon. Lett. 16 (2006) 215.
[184] J.D. Schwartz, R. Abhari, D.V. Plant, J. Azana, IEEE Trans. Microwave Theory Tech. 58 (2010) 1858.
[185] E. Hamidi, A.M. Weiner, J. Lightwave Technol. 26 (2008) 2355.
[186] E. Hamidi, A.M. Weiner, IEEE Trans. Microwave Theory Tech. 57 (2009) 890.